

2016

Characterization of the microstructural properties that are predictive of regain in strength in phosphate-deficient mice

<https://hdl.handle.net/2144/17050>

Boston University

BOSTON UNIVERSITY
SCHOOL OF MEDICINE

Thesis

**CHARACTERIZATION OF THE MICROSTRUCTURAL PROPERTIES
THAT ARE PREDICTIVE OF REGAIN IN STRENGTH IN
PHOSPHATE-DEFICIENT MICE**

by

ERIN K. SIMMONS

B.A., Boston University, 2013

Submitted in partial fulfillment of the
requirements for the degree of
Master of Science

2016

© 2016 by
Erin K. Simmons
All rights reserved

Approved by

First Reader

Louis C. Gerstenfeld, PhD.
Professor, Department of Orthopedic Surgery

Second Reader

Amira Hussein, PhD.
Postdoctoral Fellow, Department of Orthopedic Surgery

Dedication

To my father

Acknowledgments

I would like to thank Dr. Louis Gerstenfeld for allowing me to pursue research in his lab. I would also like to thank Dr. Amira Hussein for being my mentor, for investing many hours into teaching me, and for her patience. Lastly I would like to thank my family and friends for their support in my academic endeavors.

**A CHARACTERIZATION OF THE MICROSTRUCTURAL PROPERTIES THAT
ARE PREDICTIVE OF REGAIN IN STRENGTH IN
PHOSPHATE-DEFICIENT MICE**

ERIN K. SIMMONS

ABSTRACT

Fracture healing occurs in a discrete set of steps, which recapitulates embryonic endochondral bone formation. Pathophysiologies of the fracture healing that prolong the fracture repair or result in non-union may be associated with either environmental or congenital deficiencies. Phosphate deficiency resulting from either dietary or genetic perturbations can impede proper fracture healing and if prolonged can result in delayed union. The clinical assessment of regain of mechanical function is determined by measuring weight-bearing ability, palpation and various radiological approaches. These methods in general only provide qualitative evidence but are lacking in quantitative evidence of the regain in mechanical strength. The aim of this study was to characterize the microstructural properties obtained by micro-computed tomography of fracture calluses at various stages of healing and develop correlations between these structural parameters and mechanical properties that define regain of function.

Transverse, mid-diaphyseal fractures were produced on the right leg in three different murine genetic strains—A/J (AJ), C57BL/6J (B6), and C3H/HeJ (C3). Each mouse was either fed a control or phosphate deficient diet that produces a hypophosphatemic state and generates an environmental state that impairs fracture healing. Those on a phosphate deficient diet were kept on this diet for 14 days post-fracture. Fractured limbs were studied at four different post-operative time points—14, 21, 35, and 42. These four time points were based on callus stability and various phases in callus development. Contralateral limbs served as a control, representing full regain of strength. Day 0 contralateral limbs were used for the control group. Contralateral limbs were imaged and torsion tested for each strain on both control and phosphate-deficient diets. The data reveals that in regards to bone volume fraction, bone mineral density, and tissue mineral density all three strains show a progressive return to non-fractured, control values but even by post-operative day 42 do not show a 100% regain in microstructural properties. While there are interactions between specific post-operative time points and the dietary restriction, by post-operative day 42 microstructural properties showed no significant differences between the two groups, suggesting that the effects of phosphate deficiency are reversible upon a return to normal dietary conditions. The AJ and B6 strains show significant interaction between post-operative time point and dietary restrictions earlier in the fracture repair process (post-operative days 14 and 21), whereas the C3 mice show these interactions at later time points, at post-operative 35 and 42 days. Phosphate deficiency induces an overshoot in

mechanical properties at post-operative day 21 for AJ and B6 strains and at post-operative day 35 for the C3 strain that appears to be part of a process in which maximum torque and work to failure undergo a compensatory phase in which these two mechanical properties are significantly higher than in non-fractured, control limbs. The overshoot in maximum torque and work to failure is part of an adaptive process in which the callus first overshoots and subsequently returns to non-fractured control values.

These results suggest that while microstructural properties and mechanical properties are often affected by diet, this is a reversible phenomenon, which holds implications for those with phosphate deficiency due to either a metabolic or dietary disorder. If normal phosphate intake and absorption are achieved by the period at which couple remodeling is initiated (14 post-fracture) the effects on microstructural and weight bearing levels are reversible. The slower healing seen in C3 mice evidenced by the later regain in microstructural and mechanical integrity may provide a model for patients whose fractures show delayed healing in the clinic. The microstructural properties discussed have the potential to play a role in the clinic to assess fracture healing. With the advent of greater resolution CT imaging assessing these microstructural properties can be useful in determining the progression of healing.

Table of Contents

Title.....	i
Copyright Page.....	ii
Reader Approval Page.....	iii
Dedication.....	iv
Acknowledgements.....	v
Abstract.....	vi
Table of Contents.....	ix
List of Figures.....	x
List of Abbreviations.....	xii
Introduction.....	1
Materials and Methods.....	14
Results.....	23
Discussion.....	47
References.....	56
Curriculum Vitae.....	58

List of Figures

Stages of Endochondral Ossification.....	2
Radiographic Images Showing Formation of Bone and Cartilaginous Callus.....	4
3D Representations of Callus Formation and Bone Development.....	4
Variations of Microstructural Properties Across Genetic Strains in Control and Phosphate-Deficient Mice.....	6
Graphical Representation of Mechanical Properties and Osteogenic Gene Activity in C3 Mice.....	8
Schematic Demonstrating the Interdependence of Biological Processes, Microstructural Properties, and Mechanical Properties.....	10
Dependence of Mechanical Properties on Microstructural Composition.....	11
Scout View of Micro-CT Image.....	15
Representative Contoured B6 Callus.....	15
Ring Contouring.....	16
Representative 3D Rendering of Callus Ring.....	16
Potting of Superior and Inferior Ends of Femur.....	19
Schematic of Torsion Twist to Failure Technique.....	19
Torque vs. Twist Curves.....	21
Ring Bone Volume Fraction for Strains AJ, B6, and C3.....	24
Ring Bone Mineral Density for Strains AJ, B6, and C3.....	25
Ring Tissue Mineral Density in Strains AJ, B6, and C3.....	26

Ring Porosity in Strains AJ, B6, and C3.....	28
Ring Average Gap Length for Strains AJ, B6, and C3.....	29
Total Volume in Strains AJ, B6, and C3.....	30
Bone Volume in Strains AJ, B6, and C3.....	32
Bone Volume Fraction in Strains AJ, B6, and C3.....	33
Bone Mineral Density in Strains AJ, B6, and C3.....	35
Tissue Mineral Density in Strains AJ, B6, and C3.....	36
Maximum Torque in Strains AJ, B6, and C3.....	38
Work to Failure in Strains AJ, B6, and C3.....	39
Twist to Failure in Strains AJ, B6, and C3.....	41
Stiffness Narrow in Strains AJ, B6, and C3.....	43
Stiffness Break in Strains AJ, B6, and, C3.....	44
Rigidity Narrow in Strains AJ, B6, and C3.....	45
Rigidity Break in Strains AJ, B6, and C3.....	46

List of Abbreviations

A/J.....	AJ
ANOVA.....	Analysis of Variance
BMD.....	Bone Mineral Density
BMP-2.....	Bone Morphogenic Protein-2
BV.....	Bone Volume
BV/TV.....	Bone Volume Fraction
C3H/HeJ.....	C3
C57BL/6J.....	B6
Ca ²⁺	Calcium
CECT.....	Contrast-Enhanced Computed Tomography
CT.....	Computed Tomography
CtAr.....	Cortical Area
IACUC.....	International Animal Care and Use Committee
MaAr.....	Marrow Area
Ob.....	Osteoblast
Oc.....	Osteoclast
Ocyte.....	Osteocyte
Osx.....	Osterix
PBS.....	Phosphate Buffer Solution
PMMA.....	Polymethyl Methacrylate
PO ₄ ⁻	Phosphate

POD.....	Post-Operative Day
PTH.....	Parathyroid Hormone
PYD.....	Post-yield Displacement
TMD.....	Tissue Mineral Density
TtAr.....	Total Bone Area
TV.....	Total Volume

Introduction

Properties of Bone

Bone is a dynamic tissue, constantly changing and being remodeled. Aside from providing form and structure to the human body it also serves as a reservoir of minerals, such as calcium (Ca^{2+}). Bone's dynamic properties are due in part to three subsets of cells—osteoblasts, osteoclasts, and osteocytes. Because this research focuses primarily on skeletal fracture repair, this introduction to the properties of bone will cover the role of osteoblasts and osteoclasts in bone remodeling and repair. Osteoblasts participate in bone mineralization by secreting matrix vesicles whose contents include alkaline phosphatase and other enzymes whose activity raises the local concentration of phosphate (PO_4^-) (Junqueira et al. 141). Along with Ca^{2+} the phosphate ions are integral to the formation of hydroxyapatite formation, an integral part of the bone mineralization process. Osteoclasts secrete various enzymes and contain membrane associated proton H^+ pumps that are vital to the breakdown of mineralized bone tissue. These cells are sensitive to the presence of hormones, such as calcitonin, and parathyroid hormone (PTH). PTH activates osteoblasts to begin secreting the necessary stimulating factors and ligands that regulate the formation and activity of osteoclasts (Junqueira et al. 143).

Osteoporosis, a disease most commonly found in immobilized patients and postmenopausal women, results in an imbalance in which bone resorption outweighs bone formation, which ultimately results in a loss of bone mass density

(BMD). This pathophysiology is a common cause of fractures and reduced BMD is often a risk factor for developing osteoporosis.

Osteogenesis and Mechanisms of Fracture Repair

Bone growth occurs in two ways:

- 1) Intramembranous ossification in which osteoblasts differentiate directly from mesenchymal cells and begin to secrete bone matrix
- 2) Endochondral ossification in which mesenchymal cells differentiate initially into hyaline cartilage, which subsequently becomes replaced by osteoblasts, which begin to secrete osteoid leading to tissue mineralization and bone formation (Figure 1).

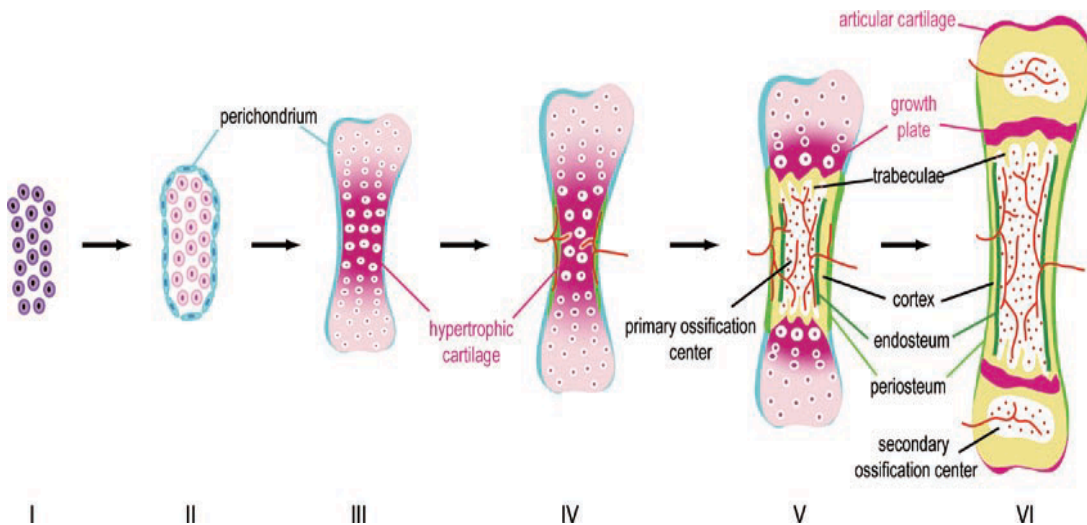


Figure 1. Stages of Endochondral Ossification. I. Mesenchymal invasion of tissue. II. Formation of cartilage template. III. Hypertrophy of chondrocytes. IV. Vascular invasion. V. Formation of primary ossification center. VI. Formation of secondary ossification center. These steps are all recapitulated during callus formation in the process of fracture repair. Figure taken from *Tissue Interactions in Long Bone Development*.

Many flat bones develop during embryogenesis via intramembranous ossification. However, a majority of bones develop through endochondral ossification, a phenomenon that has been particularly well studied in long bones.

The fractures that are currently being investigated in this study undergo a repair process whose event trajectory resembles that of endochondral development. The fracture repair process is marked by four major events:

- 1) Hematoma formation
- 2) An inflammatory phase characterized by the presence of various cytokines and macrophages to remove the debris caused by blood clots and the recruitment of mesenchymal cells to the fracture site
- 3) The proliferation and development of chondrocytes under the influence of Bone Morphogenic Protein-2 (BMP-2) to form the initial fracture callus
- 4) Mature cartilage that forms that callus is invaded by vasculature and replaced by bone (Junqueira et al. 154 and Wigner et al. 2010)

The cartilaginous callus provides the initial stability across the fracture gap as well as the template for ossification in the later stages of fracture repair. Contrast-enhanced computed tomography (CECT) analyses have demonstrated that the size of the soft callus is greatest adjacent to the fracture gap and tapers off proximally and distally with a near absence of cartilage within the fracture gap itself (See Figures 2&3). This same CECT method revealed bone formation at the proximal and distal ends of the callus and within the medullary canal (Hayward et al. 2013).

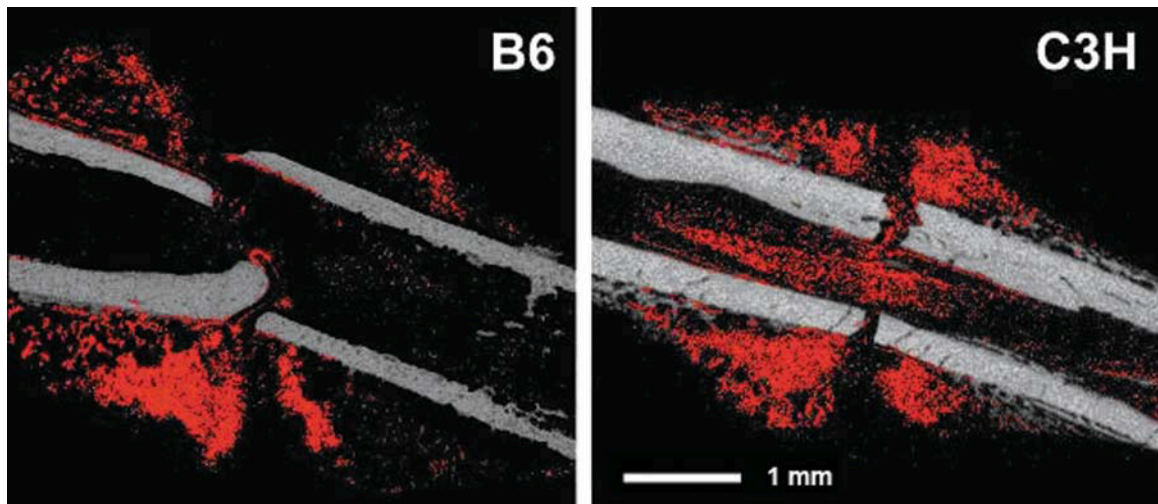


Figure 2. Radiographic Images Showing Formation of Bone and Cartilaginous Callus. Sagittal cross-sections of B6 and C3H calluses. Cartilaginous tissue is overlaid in red. Figure taken from Hayward et al. 2012.



Figure 3. 3D Representations of Callus Formation and Bone Development. Corresponding 3D representations of callus structure. Cartilage is overlaid in red and bone tissue is yellow. Figure taken from Hayward et al. 2012.

The Role of Phosphate in Bone Development and Fracture Repair

The relationship between plasma phosphate levels and parathyroid hormone (PTH) is one way in which phosphate can affect fracture repair. High plasma phosphate levels tend to stimulate the release of PTH. The net effect of constant increases of PTH on bone is to stimulate bone resorption (Boron and Boulpaep 1103); therefore, the amount of phosphate in plasma can affect fracture healing through the persistent presence of PTH. However, recently it has been discovered that *intermittent* increases in PTH levels can have the opposite effect on bone through bone deposition (Boron and Boulpaep 1103). Significant increases in mechanical properties, rates of callus formation, and callus tissue volume have all been observed in mice with daily PTH injections. The mechanism of these increases in mechanical and structural properties is primarily due to enhanced chondrogenesis in the beginning phases of callus building and fracture repair (Kakar et al. 2007). It has also been demonstrated that callus microstructural properties differ according to phosphate deficiency, which affects the strength and mineralization of the cartilaginous callus during fracture repair (See Figure 4). This phosphate deficiency affects strength and mineralization at different stages in the fracture repair process, with callus strength and toughness being higher in phosphate-deficient calluses (Hussein et al.).

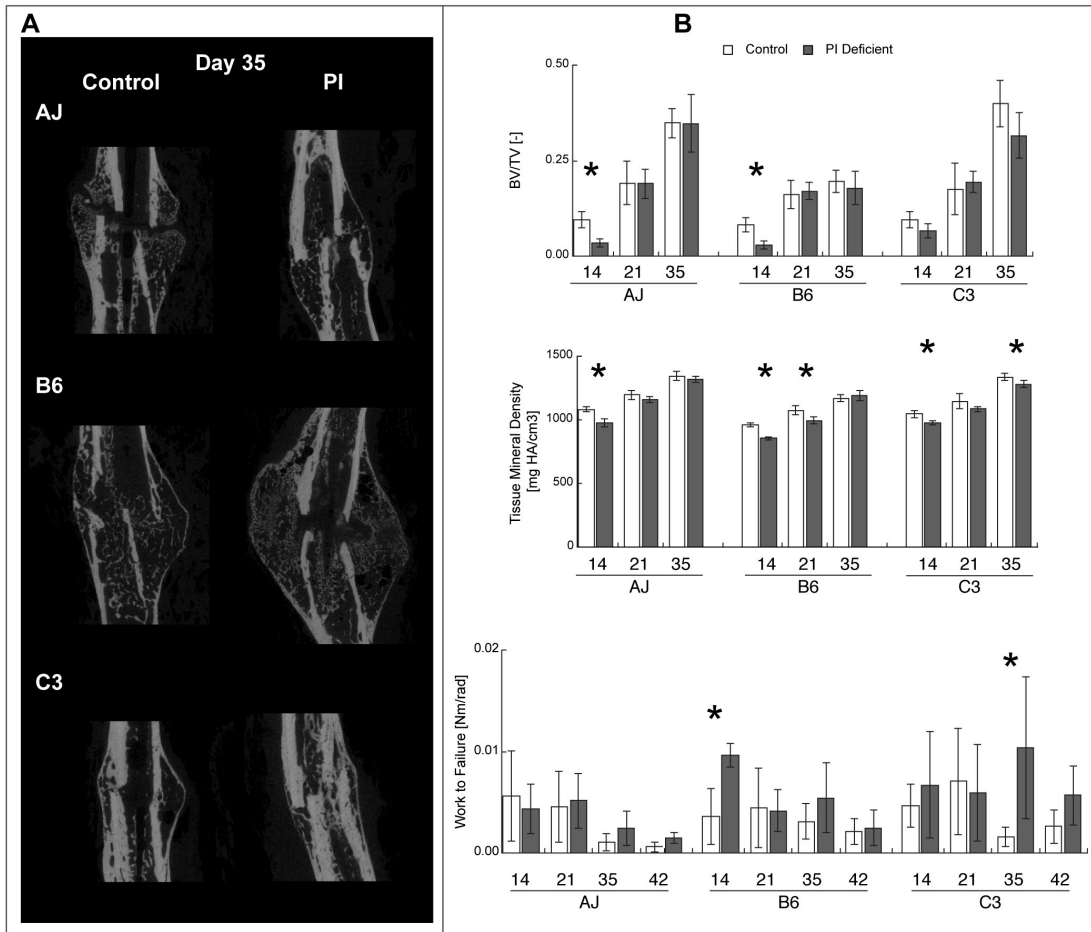


Figure 4. Variation of Microstructural Properties Across Genetic Strains in Control and Phosphate-Deficient Mice. **A.** Radiographic imaging from μ CT scans showing genetic variation in callus structure at day 35 post-fracture in both control and phosphate-deficient mice. **B.** Graphical representation of microstructural and mechanical properties of mouse femurs on control and phosphate-deficient diets. (*: Indicates significant difference between control and phosphate calluses $p < 0.05$.) Figure taken from Hussein et al 2015.

Genetic Variation and Fracture Healing

Variations in bone morphometry, fracture callus composition and healing trajectory have been found across genetic strains in mice (See Figure 4). These strains show genetic variation in bone mineral density (BMD), bone strength, bone morphology matrix/mineral composition, and trabecular architecture (Jepsen et al. 2015). These same genetic variations that have been observed in mice may also be conserved in humans, where they may underlie certain risk factors, for instance osteoporosis and other pathophysiological conditions (Parsons et al. 2005). Identifying these aspects of genetic background is of clinical significance because these traits can affect healing time and can be indicative of risk factors and thus may define when an individual may be able to resume normal weight bearing activity. Because fracture repair recapitulates endochondral bone formation rates of healing are often related to temporal patterns in chondrogenic and osteogenic lineage development and proliferation. Fracture calluses of C3 mice have demonstrated a shorter period of chondrogenesis and earlier onset of osteogenesis compared to B6 and AJ mice, which may explain the greater cross-sectional area of cortical bone observed in the C3H strain (Lybrand et al.). However, despite the rapid progression of osteogenesis the C3 strain shows slower healing than both AJ and B6 strains based on the regain of strength and stiffness (Jepsen et al. 2015). The B6 strain has shown the most prolonged period of expression for both SOX9 and SOX5, which are transcription factors whose expression is indicative of commitment and maturation of skeletal progenitor cells. This variation in expression suggests that the B6 strain undergoes

an earlier and longer period of chondrogenesis compared to AJ and C3 strains (Jepsen et al. 2015). This is in contrast to earlier osterix and RUNX2 expression in C3 mice, suggesting an earlier commitment to osteogenic differentiation in C3 (Jepsen et al. 2008). Both of these analyses indicate the variation in commitment to osteogenesis and chondrogenesis among genetic strains in mice. See Figure 5 for a graphical representation of mechanical properties and induction of gene expression in C3 mice.

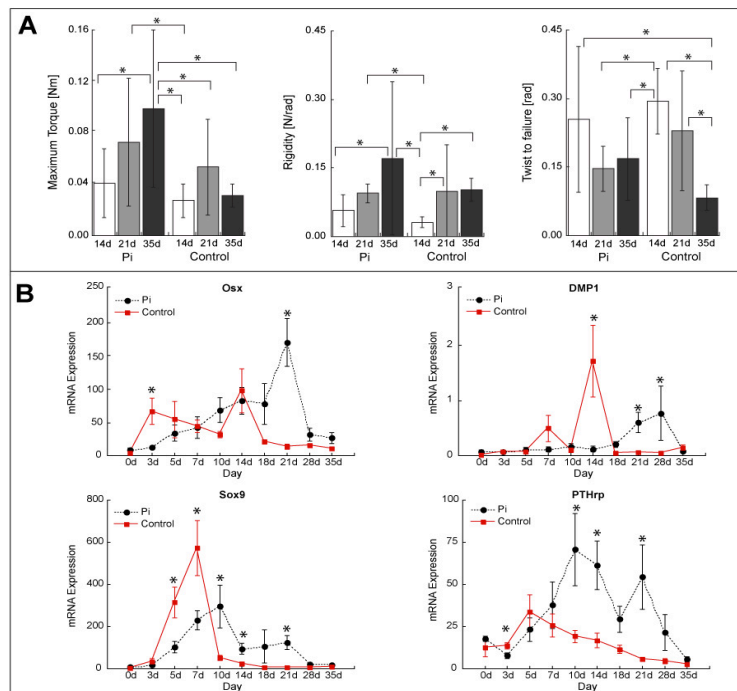


Figure 5. Graphical Representation of Mechanical Properties and Osteogenic Gene Activity in C3 Mice. A. Mechanical properties—Maximum torque, Rigidity, and Twist to failure. B. Gene expression profiles for Osx, DMP1, Sox9, and PTHrp. (*: Indicates p value < 0.05). Figure taken from Lybrand et al 2014.

Mechanical Properties of Bones

Recent understanding of the nuances in measurements of regain of strength have prompted a shift from qualitative analysis of fractured bone to quantitative analysis of regain of strength that considers brittleness, toughness, and strength. Of any micro-computed tomography (micro-CT) assessments it is the outer bridging cortices that show the greatest degree of correlation with measures of callus strength and stiffness with well fused calluses having higher breaking force than poorly fused calluses (Nyman et al. 2009). This necessitates the quantification of microstructural properties of the callus ring that encapsulates the outer bridging cortices.

A combination of μ CT evaluations and mechanical testing data reveal that phosphate deficiency affects that strength and mineralization of calluses at different stages of healing and is dependent on the strain of the mouse. Callus strength and toughness were higher in phosphate-deficient calluses indicating that although the mineral density is lower, there is a compensatory response that occurs once the phosphate has been replenished in the diet at the time point when bone formation begins to take place (Hussein, AI et al. 2014). There also exists a discrepancy between the amount of compensation that occurs once the phosphate has been replenished in the diet with the change being the most pronounced in the C3 strains (Hussein A et al. 2015). This change can be attributed to a rapid burst of osteogenic activity in the C3 strain, which utilizes proportionally more osteogenic activity than chondrogenic activity.

The following figures (Figures 6&7) summarize the connections between microstructural properties and the mechanical properties that are measured in this study. Cellular activity is connected to physical bone traits, which in turn ultimately affect the mechanical properties. Therefore, we can use imaging data (i.e. micro-computed tomography) that will give us information about the outcomes of cellular activity to elucidate correlations to regain in mechanical properties.

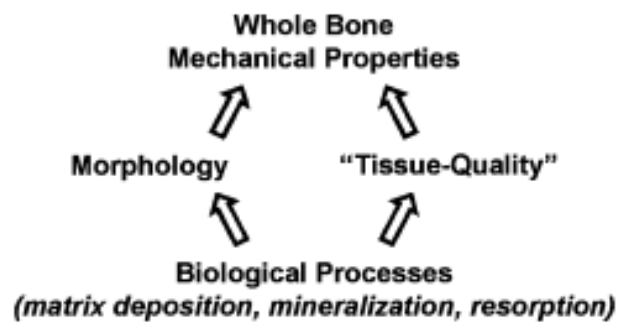


Figure 6. Schematic Demonstrating the Interdependence of Biological Processes, Microstructural Properties, and Mechanical Properties. Figure taken from Jepsen et al. 2007.

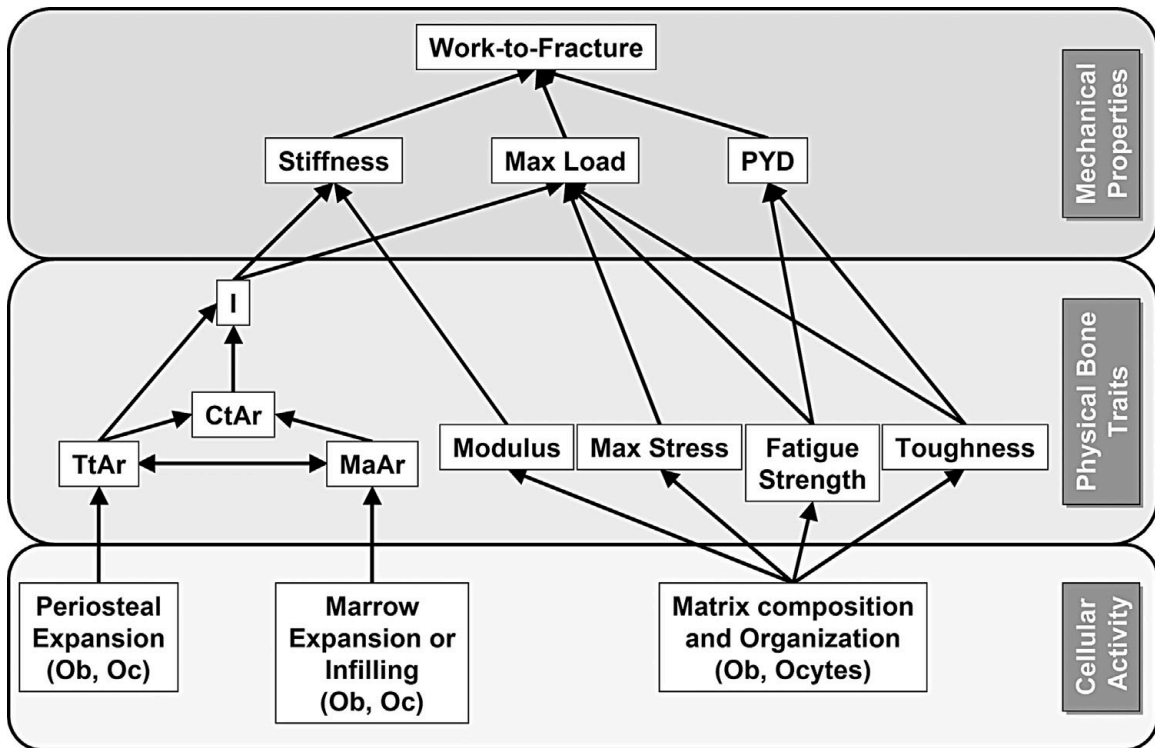


Figure 7. Dependence of Mechanical Properties on Microstructural Composition. Cellular activity influences various physical attributes of bones, which in turn influence the specific mechanical properties. Taken together these attributes link genotype to phenotype. PYD= postyield displacement; Ob= osteoblast; Oc= osteoclast; Ocyte= osteocyte; TtAr= total bone area; CtAr= cortical area; Ma.Ar= marrow area. Figure taken from Jepsen et al. 2015.

Current Study

The current study examines the effects of a phosphate-deficient diet on the regain of callus strength when compared to contralateral bones that are representative of a full regain in strength or control model. This investigation aims to interpret the effects that a phosphate-deficient diet has on the microstructural and mechanical properties in order to find correlations that can be usefully applied in clinical practice. Additionally we aim to investigate the microstructural properties of the thin 3D ring that encapsulates the outer callus cortices and to determine the

degree of bridging through examining average ring gap size and the porosity of the outer ring cortices. The three aforementioned strains were used—AJ, B6, and C3—all show variations in the patterns and rates of fracture healing. In order to examine the effects of phosphate deficiency on each strain we examined the microstructural and mechanical properties to see how differences in diet can affect the two. Time points utilized for fractured limbs include day 14, 21, 35, and 42 post-fracture. These specific time points were chosen because of the significance in the fracture healing process. Post-operative day 14 calluses were examined because this is the earliest point at which there is sufficient callus structure for mechanical testing to be feasible. Day 21 calluses were examined because it is representative of a key transition between endochondral and primary bone formation. Post-operative day 35 represents the point at which the callus has regained pre-fracture strength and is undergoing the transition to secondary bone formation and remodeling (Jepsen 2008). By post-operative day 42 the callus has been predominantly resorbed and the femur has undergone significant healing.

In conjunction with other findings, the data from this study will help to elucidate the connections between microstructural properties and mechanical strength that translate to an understanding of fracture healing and certain pathophysiological states. There were three specific objectives of this study:

- 1) Use micro-computed tomography to assess the effect of post-operative day and diet on average gap size in the outer ring and porosity throughout the callus.

- 2) Measure the relative regain of microstructural properties and strength using contralateral (non-fractured) limbs as a reference.

Materials and Methods

Murine Surgical Model

All animal research that was conducted conformed to IACUC protocols. Unilateral, mid-diaphyseal pinned fractures were produced on the right femur of B6, AJ, and C3 male mice using a modification of the blunt guillotine procedure first outlined on rats in Bonnarens and Einhorn (Bonnarens and Einhorn, 1985) and subsequently modified for mouse (Jepsen et al 2008). Radiographic images were obtained immediately after fracture to confirm the presence of a mid-shaft, stabilized fracture with minimal comminution. The phosphate deficient diet was introduced two days prior to fracture and was maintained for 14 days. After this period phosphate was re-introduced into the diet and continued until 21, 35, and 42 days post-fracture. Control mice were fed a normal diet.

μCT Scanning and Image Processing

All femora were scanned using a voxel size of 12 μm (70 kVp, 114 μA; μCT 40, Scanco Medical, Brüttisellen, Switzerland). Fractured limbs with calluses were scanned such that the entire callus was included in the section. The non-fractured, contralateral limbs were scanned at the mid-diaphyseal region (309 slices; 3.7 mm). See Figure 8.



Figure 8. Scout View of Micro-CT Image. Two femurs stacked vertically. The two horizontal lines on the bottom femur are the start and stop points for the scanner. The area in this image is the area taken up by the fracture callus. In non-fractured femora the region was uniformly distributed into 309 slices, equivalent to 3.7 mm at the mid-diaphysis. Figure taken from A. Wulff, 2015.

Micro-CT Analysis of 3D Ring Callus Microstructural Properties

In order to include only the region of interest (i.e. callus and cortical bone) the image was traced using the same Scanco software that was used to scan the micro-CT images (Figure 9).

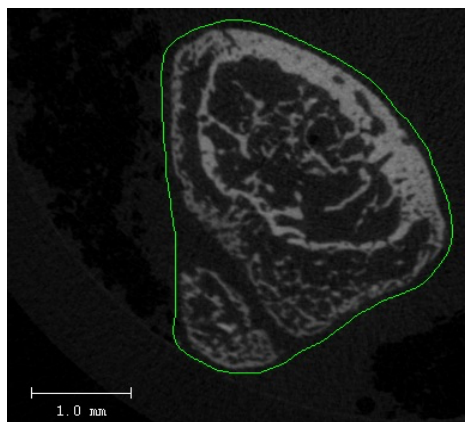


Figure 9. Representative 2D Contoured B6 Callus.

To ensure that only the bridging cortices were included the original outer tracing was shrunk to create an inner contour (Figure 10). 3D renderings of contouring can be seen in Figure 11.

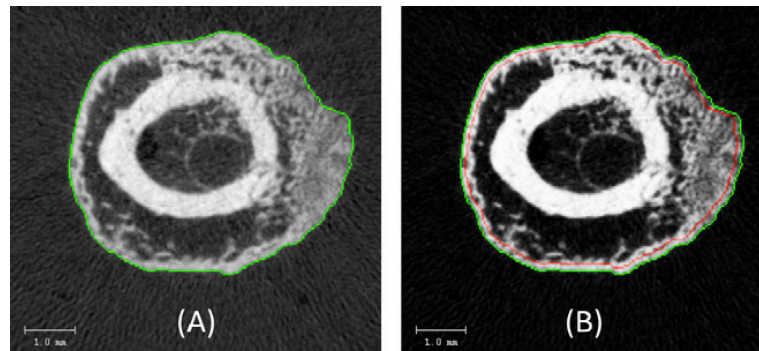


Figure 10. Ring Contouring. A) Outer cortex. B) 3D callus ring is contoured. Figure taken from Nyman et al. 2009.

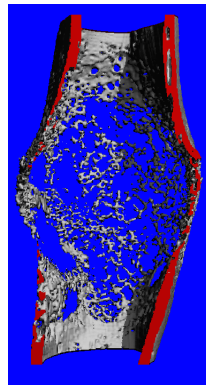


Figure 11. Representative 3D Rendering of Callus Ring. Frontal view after digitally removing half of the callus.

Only voxels obtained from micro-CT images that exceeded 45% of the average intensity of pre-existing bone were included. These threshold values differed according to the strain with A1 having the highest threshold at 27.4% of maximum gray scale intensity, followed by C3 at 26.3%, and B6 at 24.7%. An analysis of the 3D ring that is the callus surface included evaluations of the following

microstructural properties. Note that the 3D ring analysis excluded the measurements of total volume and bone volume.

- Total Volume (TV), defined as the total volume of the entire callus including the cortical bone and marrow cavity.
- Bone Volume (BV), defined as the volume of voxels that exceed a predetermined threshold of 45% of the average intensity of pre-existing bone.
- Bone Volume Fraction (BV/TV), defined as the relative amount of voxels that exceed 45% of the average intensity of pre-existing bone.
- Average gap size, defined as a measurement of the average size of individual gaps in trabecular bone that exist within a ring around the callus.
- Porosity, defined as the total amount of space not occupied by bone tissue exceeding 45% of the average intensity of pre-existing bone. Porosity was calculated using the following equation:
$$\frac{TV-BV}{TV} \text{ or } 1 - \left(\frac{BV}{TV}\right).$$
- Bone Mineral Density (BMD), defined as the average intensity of all the voxels within the given region of interest. This includes unmineralized soft tissue, bone, and marrow space.
- Tissue Mineral Density (TMD), defined as the average intensity of mineralized tissue within the callus.

Regain in Microstructural Properties

The following microstructural properties were compared to day 0 non-fractured control femora: Total Volume (TV), Bone Volume (BV), Bone Volume Fraction (BV/TV), Bone Mineral Density (BMD), and Tissue Mineral Density (TMD). All absolute values obtained were averaged and divided by the average of day 0 control femora to obtain the relative regain in microstructural properties.

Mechanical Testing

Following each scan the femurs were subjected to mechanical testing via the torsion testing system (MT55, Instron, Norwood, MA). Each of the proximal and distal ends of the femurs was secured using polymethyl methacrylate (PMMA) in 10x10mm² aluminum cubes. Adequate hydration of the samples during testing was maintained by immersing the bones in PBS up until they were tested. When potted the samples were manually maintained in an aligned position along their diaphysis until the PMMA had hardened (Figure 12). The callus center was fixed in the testing apparatus such that it remained equidistant from both the proximal and distal portions of the potted ends. The gauge length was the average of four measurements taken at 90° increments around the cube. The samples were then held securely in the testing machine by securing the potted ends within the claw grips and tightening thumbscrews (Figure 13). Angular displacement was applied at 0.5° increments until failure occurred.



Figure 12. Potting of Superior and Inferior Ends of Femur.
Figures taken from A. Wulff, 2015.

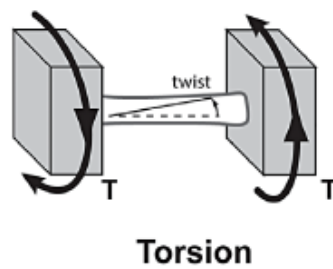


Figure 13. Schematic of Torsion Twist to Failure Technique. Rotational equivalent of force.
Figure taken from Jepsen et al. 2015.

Mechanical failure is defined as the point at which the diaphysis or fracture callus has re-fractured. This point can be observed both visually by seeing the sample fracture and by observing the torsion curve in which mechanical failure is graphically represented as a peak after which angular displacement immediately falls toward zero in the torsion curve. The following mechanical properties were analyzed to determine regain in functionality of bone:

- Maximum torque
- Work to Failure
- Stiffness
- Rigidity
- Twist to Failure

Maximum torsional strength was defined as the maximum torque sustained by the sample. Work to failure is the area under the load-deformation curve and takes into account both the stiffness and the maximum torque sustained by the sample. Twist to failure was defined as the angular displacement sustained by the bone at maximum torque. Torsional rigidity is measured as the slope of the linear portion of the torsion vs. twist curve (Morgan et al. 2009) and is defined as the stiffness. Stiffness and rigidity were measured using two measurements. The first, which will be referred to as “narrow” uses only the linear portion of the torsion vs. twist curve (Figure 14). The other measurement is “break” which utilizes the entire curve up to the point of failure, which includes the yield point. Because the linear portion is not always readily apparent we wanted to minimize user differences so the “narrow” and “break” measurements were both obtained. The twist value was

normalized by gage length in rigidity measurements. All measures of mechanical strength were quantified from the load-deformation curves using MatLab scripts.

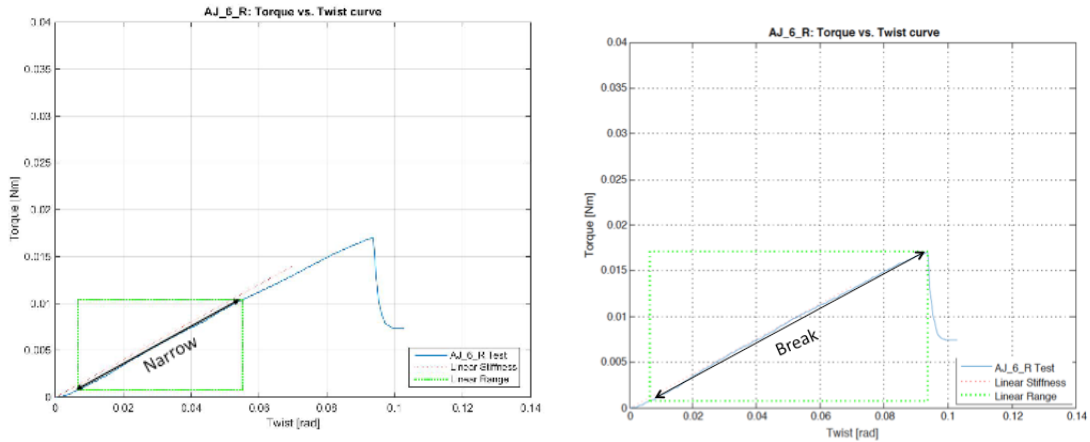


Figure 14. Torque vs. Twist Curve. Peak is maximum torque sustained by sample. Slope is stiffness. Green rectangle represents “narrow” region. “Break” region extends to peak at maximum torque. Figures taken from A. Wulff, 2015.

Statistical Analysis

A two-factor ANOVA test was performed to test for significant differences within genetic strains between the two experimental conditions—diet, and post-operative time point. Tukey post hoc analysis was used to find statistical differences in measurements taken at different post-operative time points as well as statistically significant interactions between diet and post-operative day. A student's t-test was used to determine statistical significance in differences between the control and phosphate-deficient groups ($p < 0.05$).

Results

Analysis of External Ring of Microstructural Properties

While prior studies have focused on whole callus microstructural properties and their relationship to the regain in mechanical function, these properties by themselves fail to quantitatively assess the bridging of the fracture gap. This aspect of fracture repair is one of the key structural features in the regain of mechanical integrity of fracture healing and is used clinically to assess the ability to bear weight. In order to determine if this feature of fracture callus repair can be assessed, micro-CT measurements were made for a defined outer ring of mineralized tissue inside the callus perimeter to assess if these measurements could be used to quantitatively capture this structural feature of repair and if it would provide a good correlation to the regain in strength.

Figures 15, 16 and 17 show the analysis of the total bone volume, bone mineral density and total mineral density tissue in this outer ring of bone, for each of the three strains at four times of analysis, in control and Pi-deficient diet fed mice. These micro-CT analyses show statistically significant differences across the total post-operative time course for the control calluses. Diet as a separate factor had very selective differences however that were strain specific. The control animals for all three strains showed a time dependent statistically significant increase for both the total bone volume and bone mineral density. Interestingly total tissue mineral density showed a clear difference in that the first two time points which were significantly lower than the latter two time points. In relationship to the effect of

dietary deficiency in phosphate both AJ and B6 strains showed strong interactions with diet specifically reflected in specific changes seen at the earliest time points.

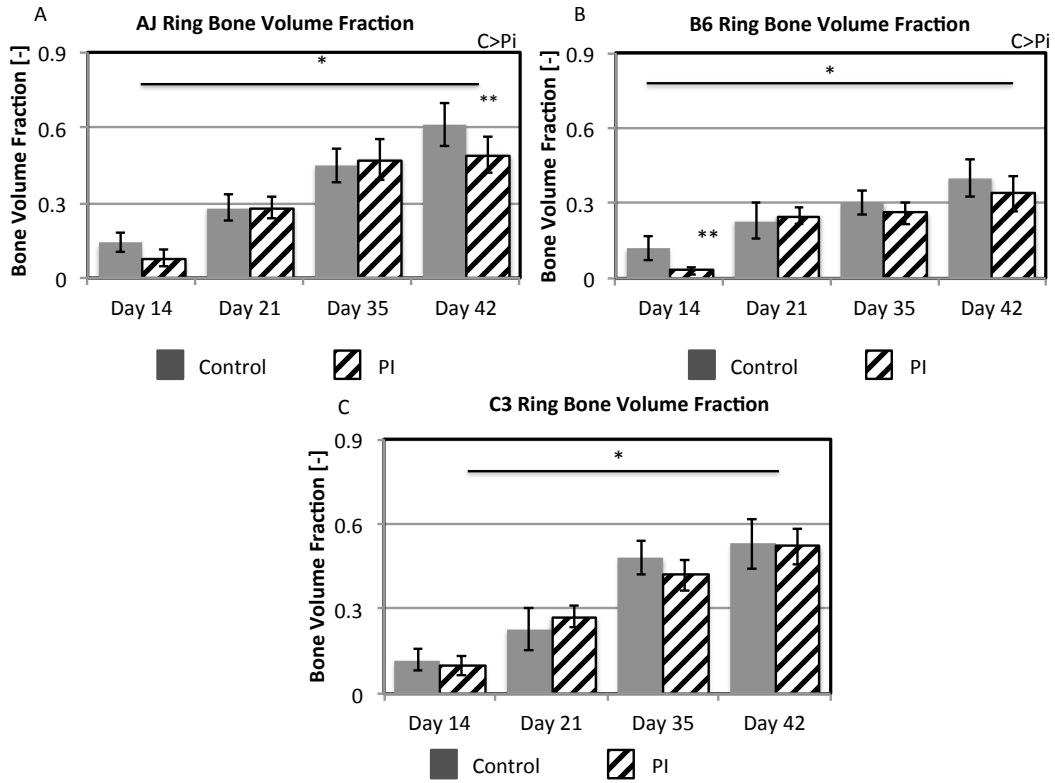


Figure 15. Ring Bone Volume Fraction for Strains AJ, B6, and C3. A,B,C) * above horizontal lines signifies an interaction with POD. Significantly different results in POD are separated by vertical lines. ** above specific day signifies an interaction between POD and diet.

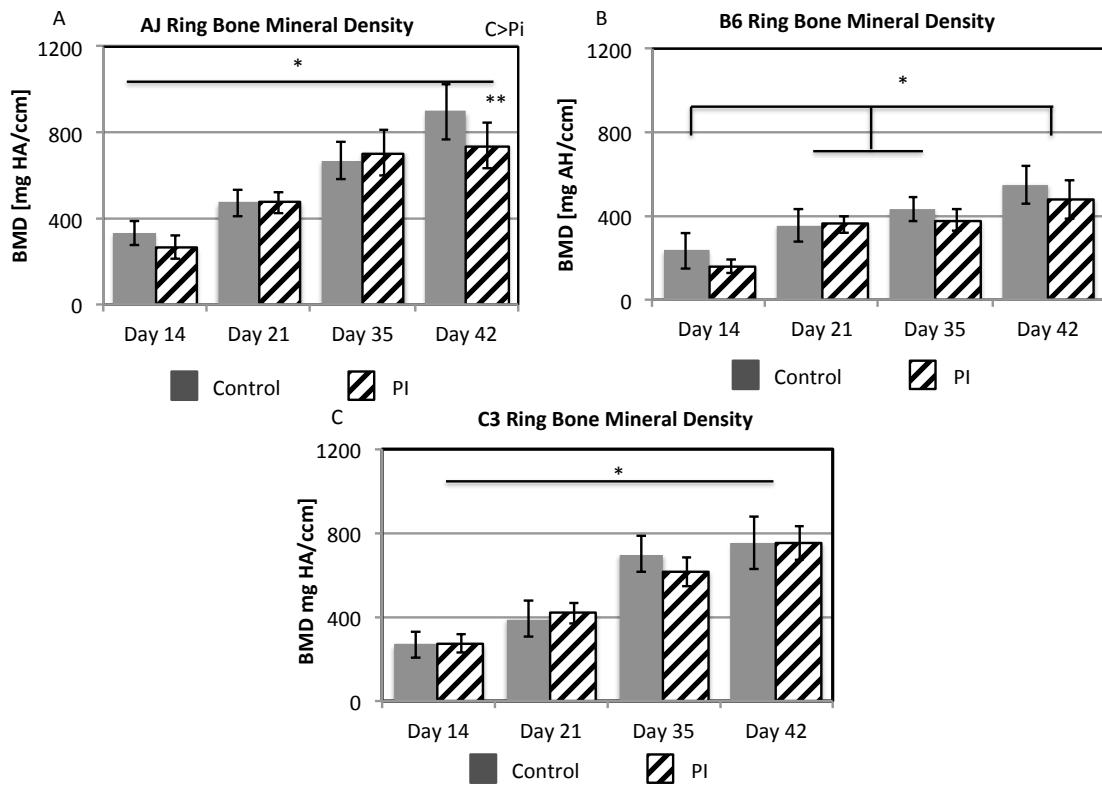


Figure 16. Ring Bone Mineral Density for Strains AJ, B6, and C3. A,B,C,)* above horizontal lines signifies an interaction with POD. Significantly different results are separated by vertical lines. Significant difference due to diet alone is indicated on figure. ** above specific day signifies an interaction between POD and diet.

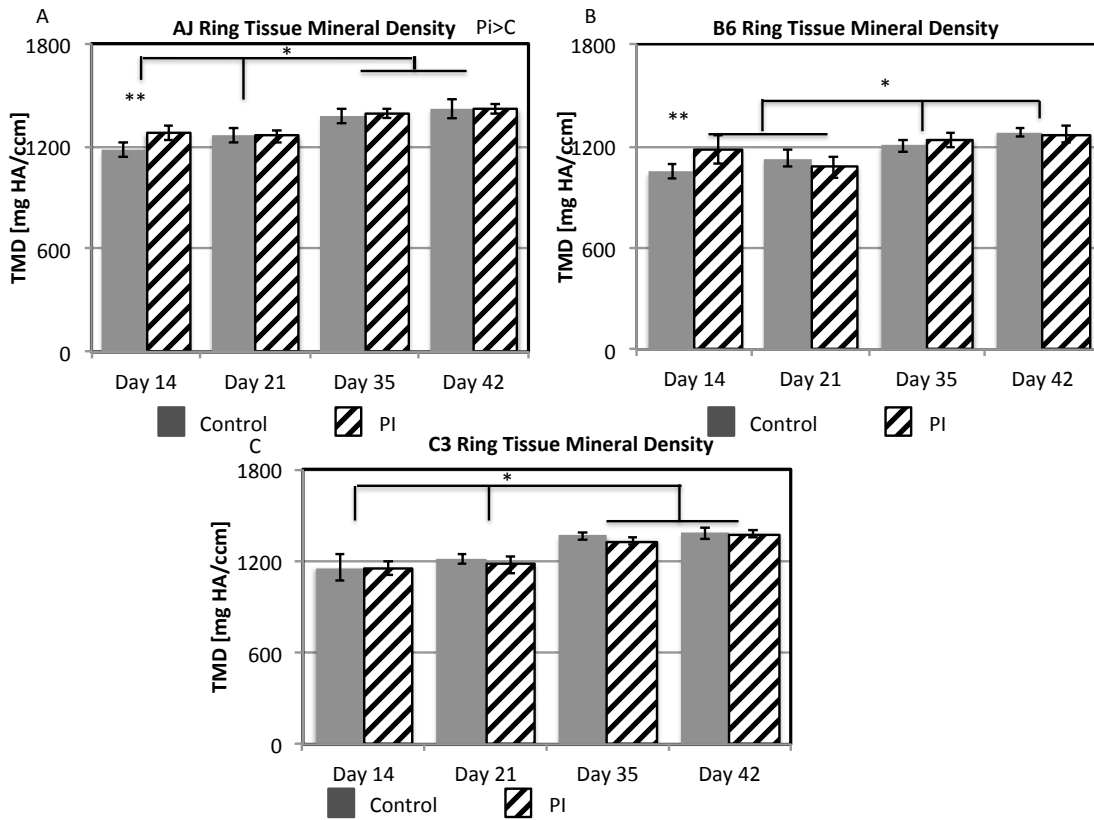


Figure 17. 3D Ring Tissue Mineral Density in Strains AJ, B6, and C3. * above horizontal lines signifies an interaction with POD. Significantly different results are separated by vertical lines. Significant difference due to diet alone is indicated on figure. ** above specific day signifies an interaction between POD and diet.

The structural aspects of the bridging of the fracture gap was measured by assessing both the porosity of the callus ring (Figure 18) and the measurement of the callus gap (Figure 19). All three strains showed an inverse and statistically significant diminishment in porosity over the healing period that was examined. In contrast the average gap length showed statistically significant and complete closure in length between days 14 and 21. A comparison of these parameters between the control and Pi diet deficient mice of that porosity showed good correlation with the differences seen for total bone volume and BMD.

Interestingly the one feature that correlated best to the diet deficiency in the three strains was differences gap length. The average gap length, which was defined as the average length of individual gaps in between trabeculae of bone. Only POD 14 was statistically significant from POD 21, 35, and 42 with POD 14 having the greatest average gap length, which was significant for all three strains. Overall all time points for the B6 and C3 strains there was no statistically significant diet effect on average gap length, but there was an interaction between time and diet at POD 14 for the AJ mice largely due to the very large size of the gap at 14 days that was observed in this strain.

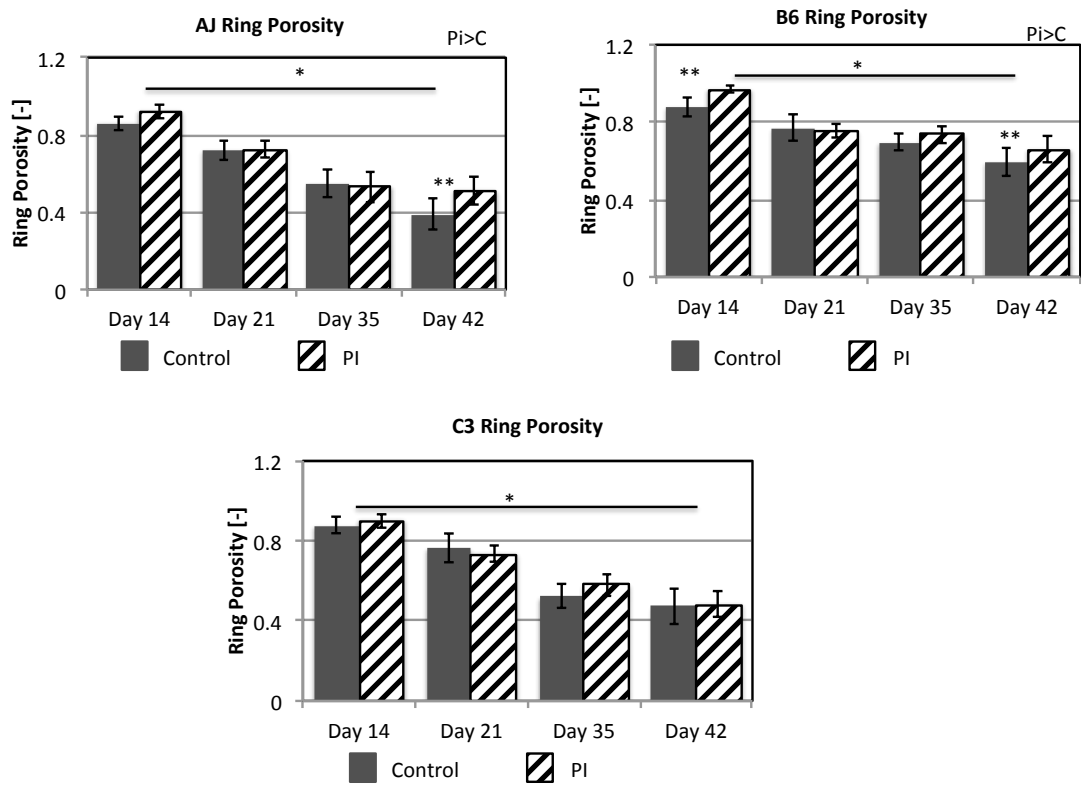


Figure 18. Ring Porosity in Strains AJ, B6, and C3. A,B,C) * above horizontal lines signifies an interaction with POD. Significantly different results are separated by vertical lines. Significant difference due to diet alone is indicated on figure. ** above specific day signifies an interaction between POD and diet.

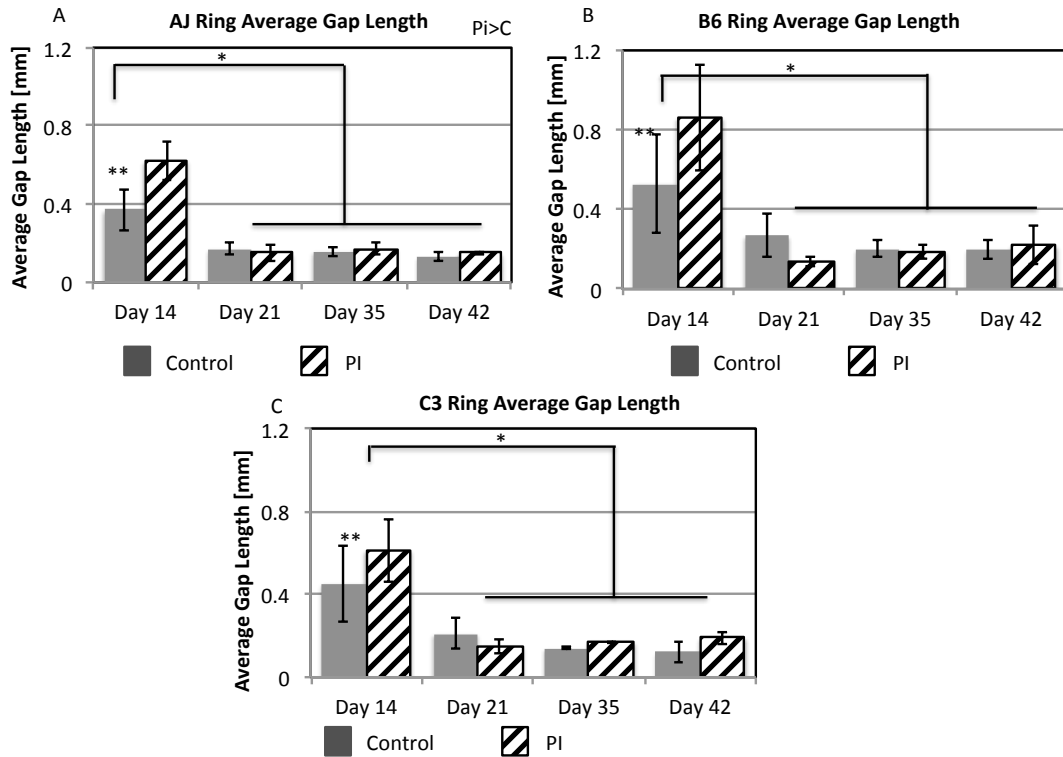


Figure 19. Ring Average Gap Length for Strains AJ, B6, and C3. A,B,C,)* above horizontal lines signifies an interaction with POD. Significantly different results are separated by vertical lines. Significant difference due to diet alone is indicated on figure. ** above specific day signifies an interaction between POD and diet.

Regain in Whole Callus Microstructural Integrity

The next part of these studies focuses on the microstructural changes within the whole callus and places these in context to the regain in mechanical strength. The following figures of microstructural properties are demonstrated as percentages of control, non-fractured limbs. This is a reflection of the relative

regain of microstructural properties back to an original pre-fracture state.

Summaries of all of these data are presented in Figures 20 -24.

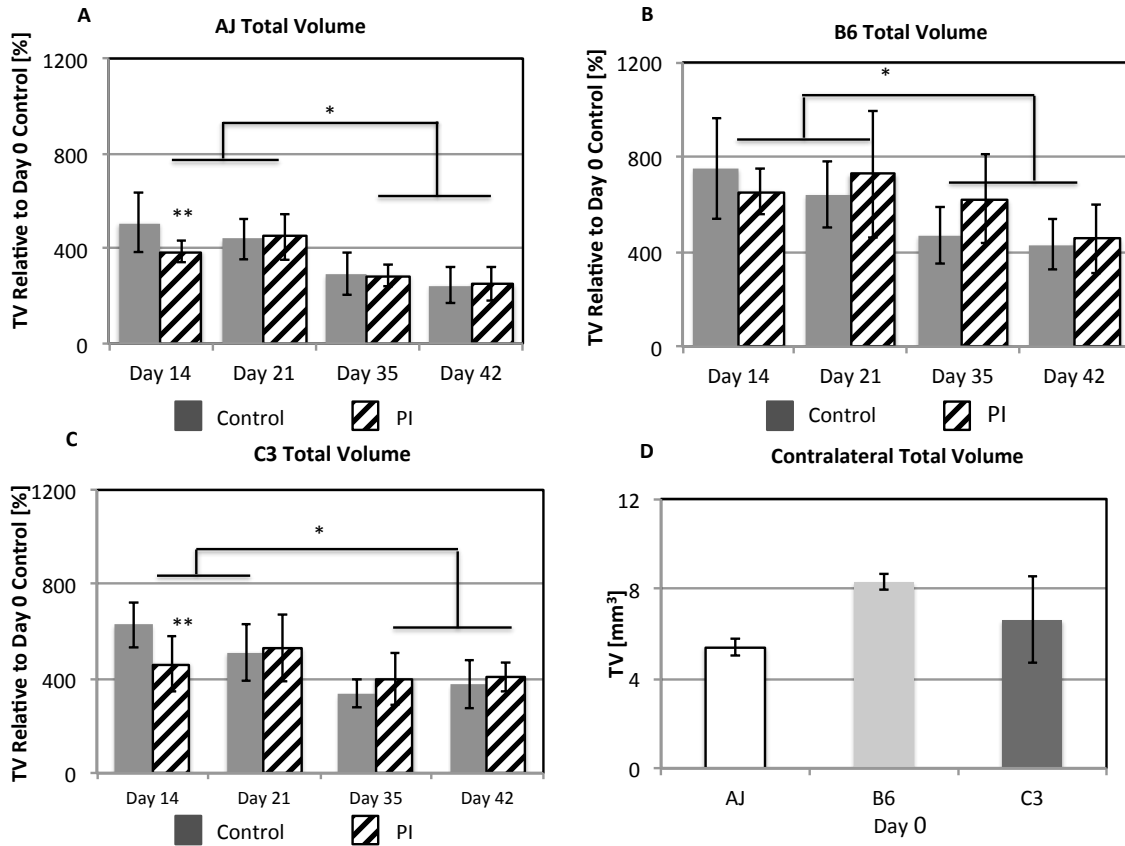


Figure 20. Total Volume of Strains AJ, B6, and C3. A,B,C) All values are plotted as percentages of Day 0 control, non-fractured mice femora. Contralateral values are included as a reference. * above horizontal lines signifies an interaction with POD. Vertical lines separate significantly different results. ** above specific day signifies an interaction between POD and diet. D) Contralateral limb values at day 0 for total volume.

For all strains of mice the two earlier time points show significantly higher total volume compared to POD 35 and POD 42 (Figure 20). The only significant difference in diet effects was seen at POD 14, which was seen in both the AJ and C3 strains but was not in the B6 mice. Overall differences in bone volume and the bone volume fraction are presented in Figures 21 and 22. Overall the total volume of bone increased until 21 days with these two earlier times being significantly different from either of the later times points for all of the strain. On the other hand as healing progressed and the callus was remodeled the bone fracture volume steadily increased with both later time points being significantly higher than the early time points in AJ and C3 strains. In contrast the bone fraction in the B6 calluses did not significantly change after 21 days (Figure 22).

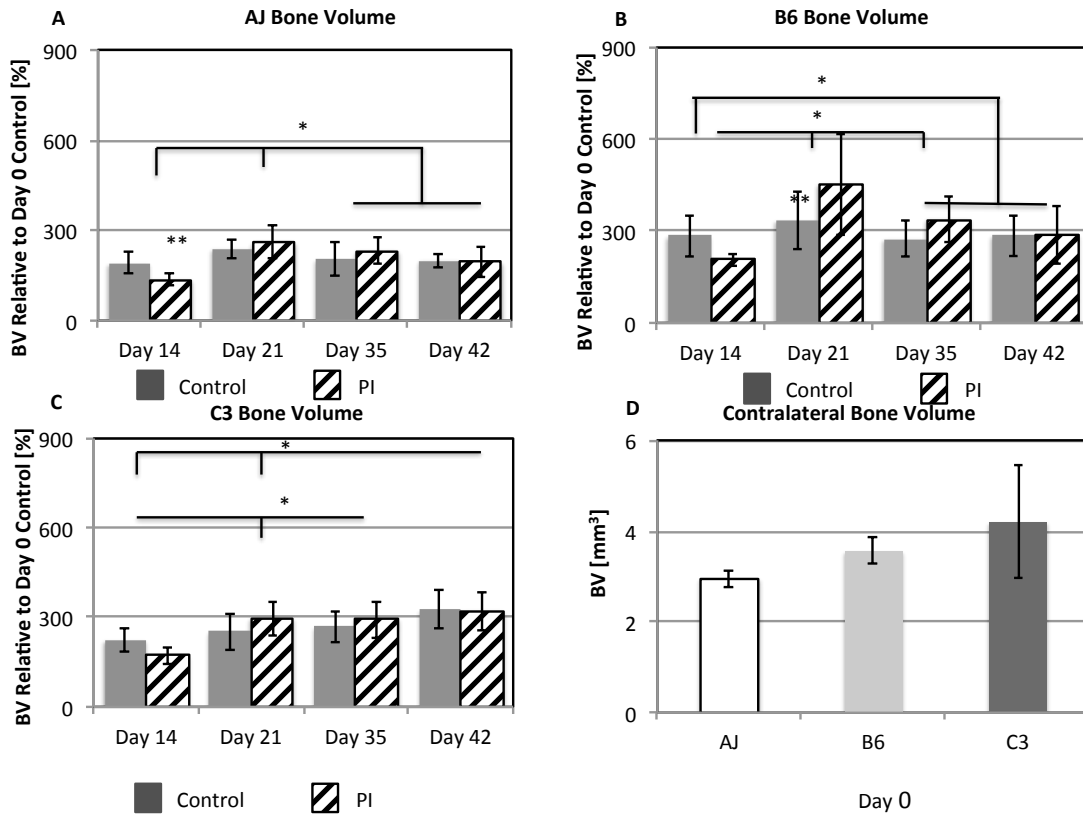


Figure 21. Bone Volume in Strains AJ, B6, and C3. All values are plotted as percentages of Day 0 control, non-fractured mice femora. Contralateral values are included as a reference * above horizontal lines signifies an interaction with POD. Significantly different results are separated by vertical lines. ** above specific day signifies an interaction between POD and diet. D) Contralateral limb values at day 0 for bone volume.

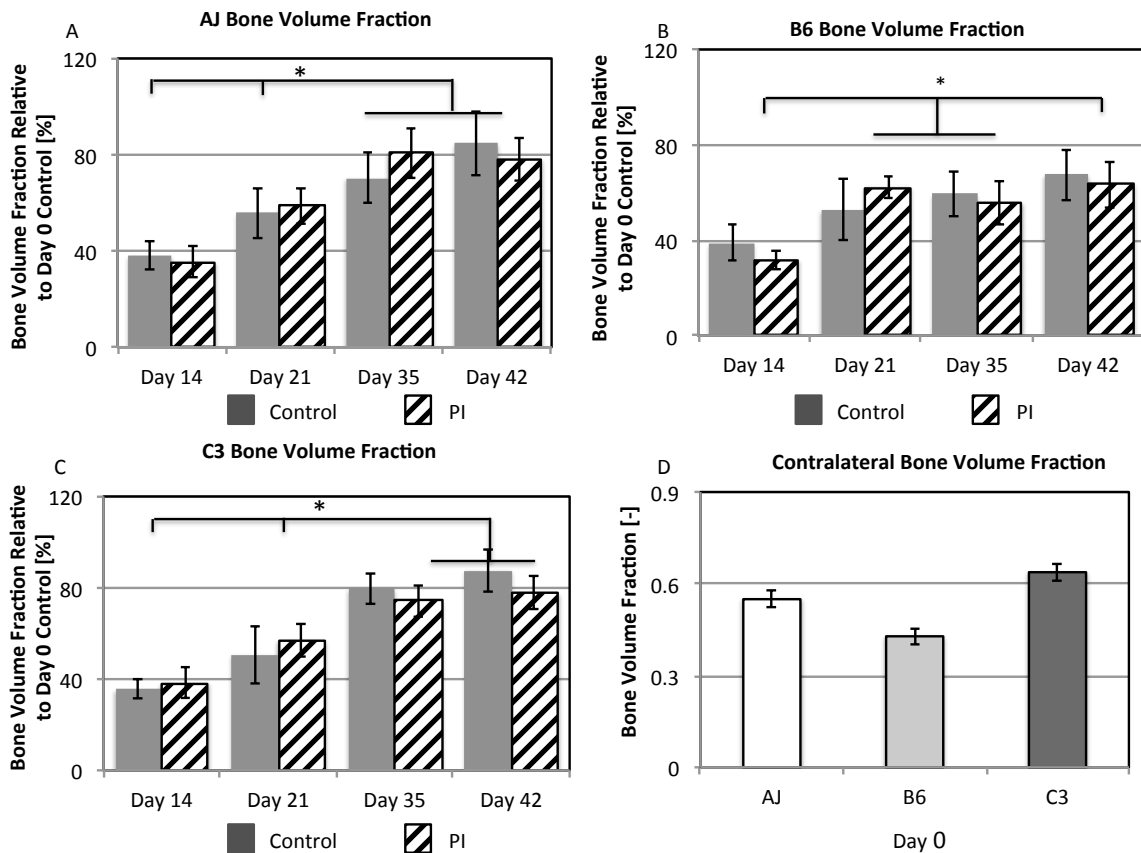


Figure 22. Bone Volume Fraction in Strains AJ, B6, and C3. A,B,C) All values are plotted as percentages of Day 0 control, non-fractured mice femora. Contralateral values are included as a reference * above horizontal lines signifies an interaction with POD. Significantly different results are separated by vertical lines. D) Contralateral limb values at day 0 for bone volume fraction.

A comparison of the effect that dietary Pi restriction had on these aspects of callus structure showed once again that only selective time points were significantly different with both the AJ and C3 calluses showing smaller total callus and bone volumes while the B6 mice had significantly larger calluses and bone volumes at day 21.

The final two aspects of whole callus structure that were examined are Bone Mineral Density and Total Mineral Density (Figures 23 and 24). In all strains there is a trend of increasing mineral density across time in both BMD and TMD measurements and by POD 42 all strains have achieved approximately 100% regain in mineral density properties. AJ and B6 show always show a significant difference in mineral density between POD 14 and POD 42. However, the C3 strain is notable for its trajectory in changing mineral density because all time points for both BMD and TMD show significant differences. BMD shows no effects due to diet. Dietary effects are only seen in TMD measurements in the B6 and C3 strains (Figure 24). In both B6 and C3 mice the Pi-deficient group shows greater TMD. B6 mice are the only strain that show an interaction between diet and time. This occurs at POD 14 at which point the Pi-deficient mice have greater TMD than control mice.

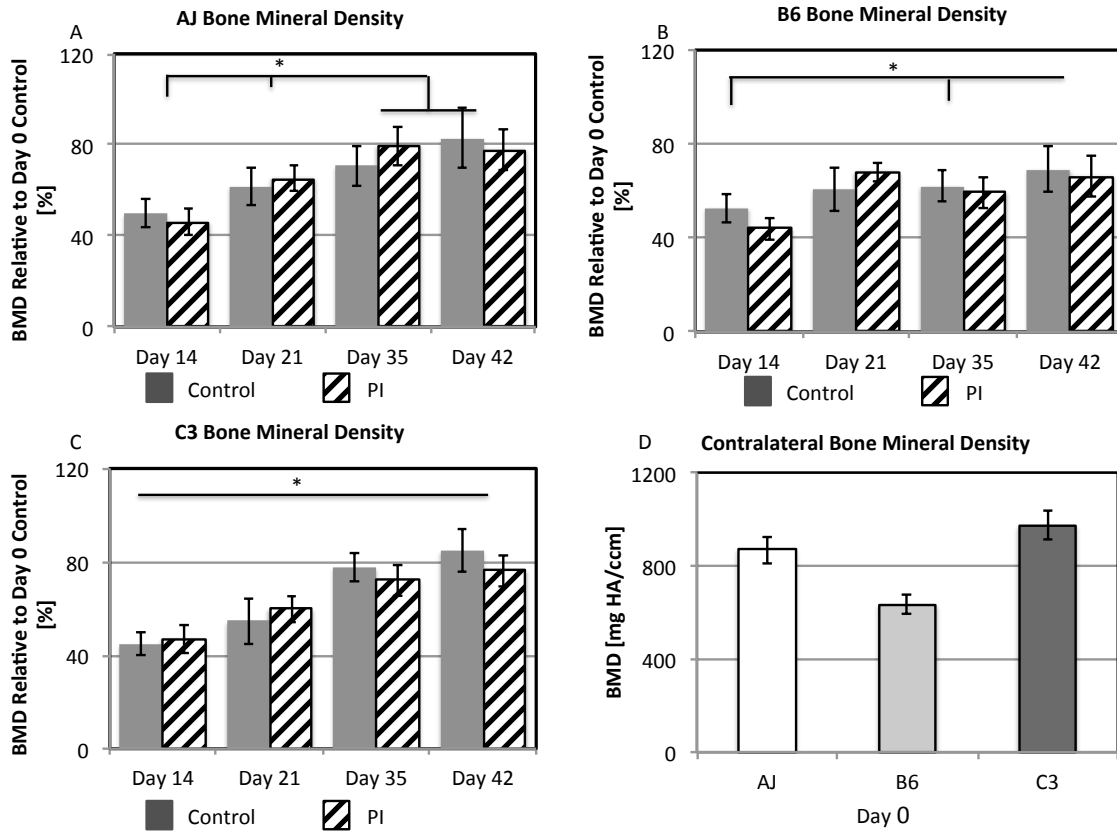


Figure 23. Bone Mineral Density in Strains AJ, B6, and C3. A,B,C) All values are plotted as percentages of Day 0 control, non-fractured mice femora. Contralateral values are included as a reference. * above horizontal lines signifies an interaction with POD. Significantly different results are separated by vertical lines. D) Contralateral limb values at day 0 for bone mineral density.

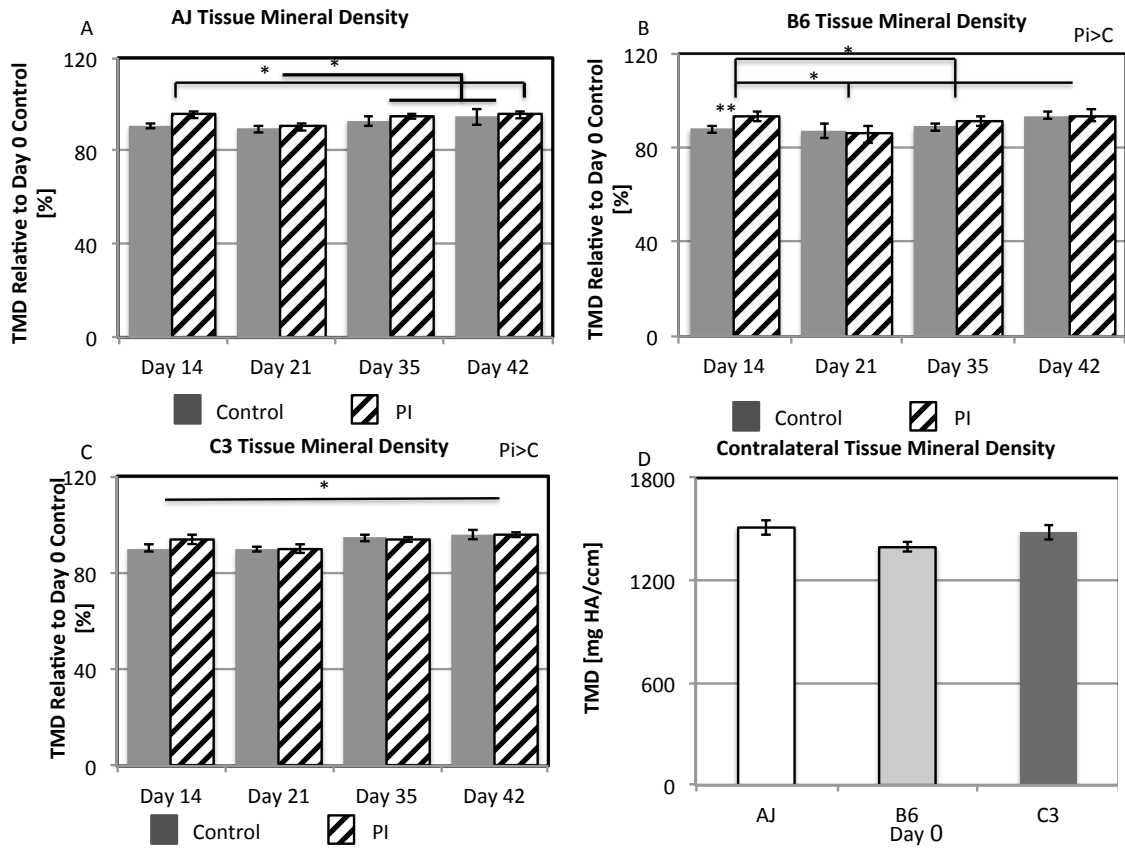


Figure 24. Tissue Mineral Density in Strains AJ, B6, and C3. All values are plotted as percentages of Day 0 control, non-fractured mice femora. Contralateral values are included as a reference. * above horizontal lines signifies an interaction with POD. Significantly different results are separated by vertical lines. Significant differences due to diet effects are indicated on figure. ** above specific day signifies an interaction between POD and diet.

Regain in Mechanical Function

The final part of this study examines whole bone mechanical properties. As previously demonstrated in the regain in whole callus microstructural integrity these mechanical test results are presented as a percentage of control, non-fractured limbs. These are measurements of the relative regain in mechanical properties back to an original pre-fracture state. A summary of all these data is provided in figures 25-31. Overall mechanical integrity of bone requires quantifying aspects of bone strength, toughness, and stiffness. These results reveal that if there is a dietary effect on mechanical properties Pi-deficient mice have the greater value of mechanical function.

Maximum torque is a measure of the mechanical strength of bone and is represented in Figure 25. In AJ and B6 strains maximum torque is greater than control, non-fractured limbs, peaking at POD 21, at which point in time the volume is greatest. By POD 35 and POD 42 the maximum torque of AJ and B6 bones returns to approximately 100% of control, non-fractured values. The C3 mice show a somewhat different trajectory with a peak in maximum torque at POD 35. However, the C3 mice—like the AJ and B6 mice—return to approximately 100% of control, non-fractured values by POD 42. Overall dietary effects on maximum torque were only seen in C3 mice where Pi-deficient mice have a significantly higher maximum torque than control mice. Dietary effects at specific time points are seen in both AJ and C3 mice, but these effects are seen at different points in time. In AJ mice this interaction is earlier at POD 21 and in C3 mice this interaction occurs later at POD

35. All dietary interactions in mice reveal that Pi-deficient mice in both AJ and C3 mice have greater maximum torque than control mice. B6 mice show no dietary influence on maximum torque.

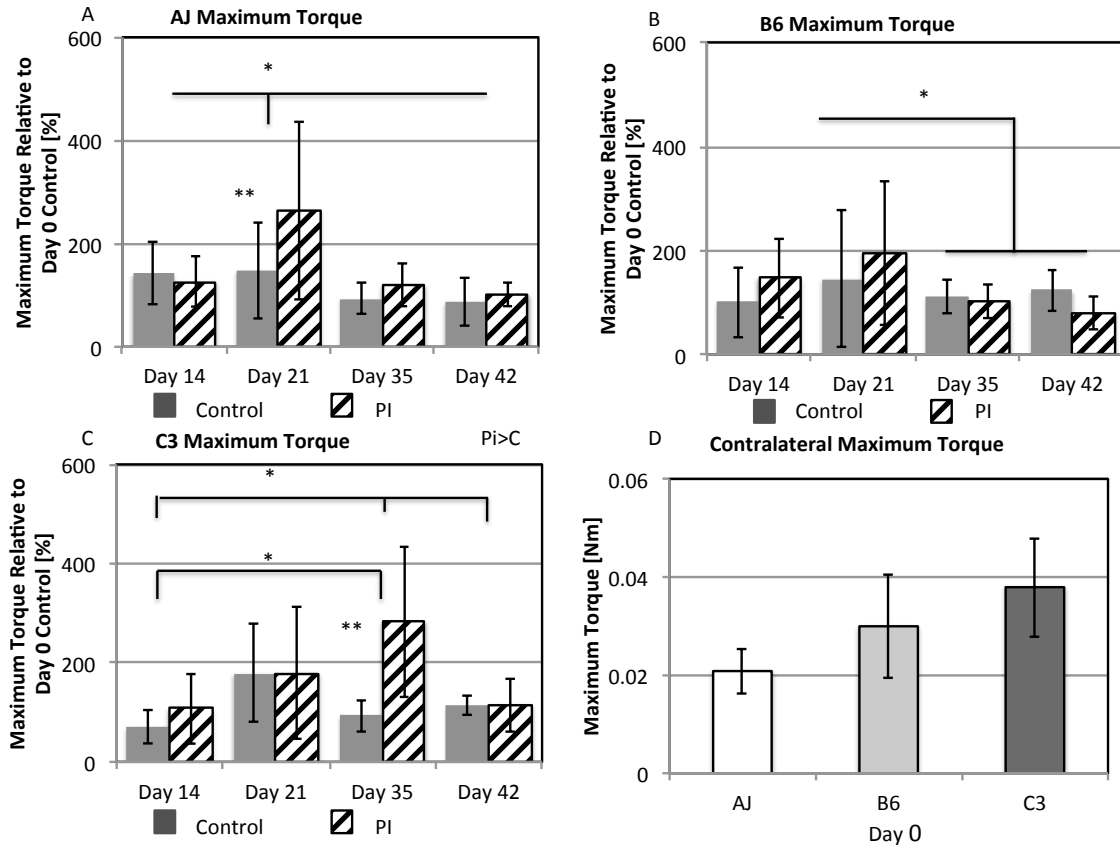


Figure 25. Maximum Torque in Strains AJ, B6, and C3. All values are plotted as percentages of Day 0 control, non-fractured mice femora. Contralateral values are included as a reference. * above horizontal lines signifies an interaction with POD. Significantly different results are separated by vertical lines. Significant differences due to diet effects are indicated on figure. ** above specific day signifies an interaction between POD and diet.

Work to failure is the measure of toughness and is shown in Figure 26. In AJ and B6 mice work to failure changes across time with earlier time points having greater work to failure than later time points. In all strains work to failure shows an

approximately 100% return to control, non-fractured values by POD 42. Dietary effects are variable among strains. AJ mice show no dietary effects on work to failure, but in both B6 and C3 mice Pi-deficient mice have a greater work to failure than control mice. Specific time points at which a dietary interaction is seen are variable between B6 and C3 mice. B6 mice show an earlier dietary interaction on work to failure than C3 mice. In the B6 strain work to failure is significantly greater in Pi-deficient mice at POD 14. C3 mice show this same interaction but at POD 35.

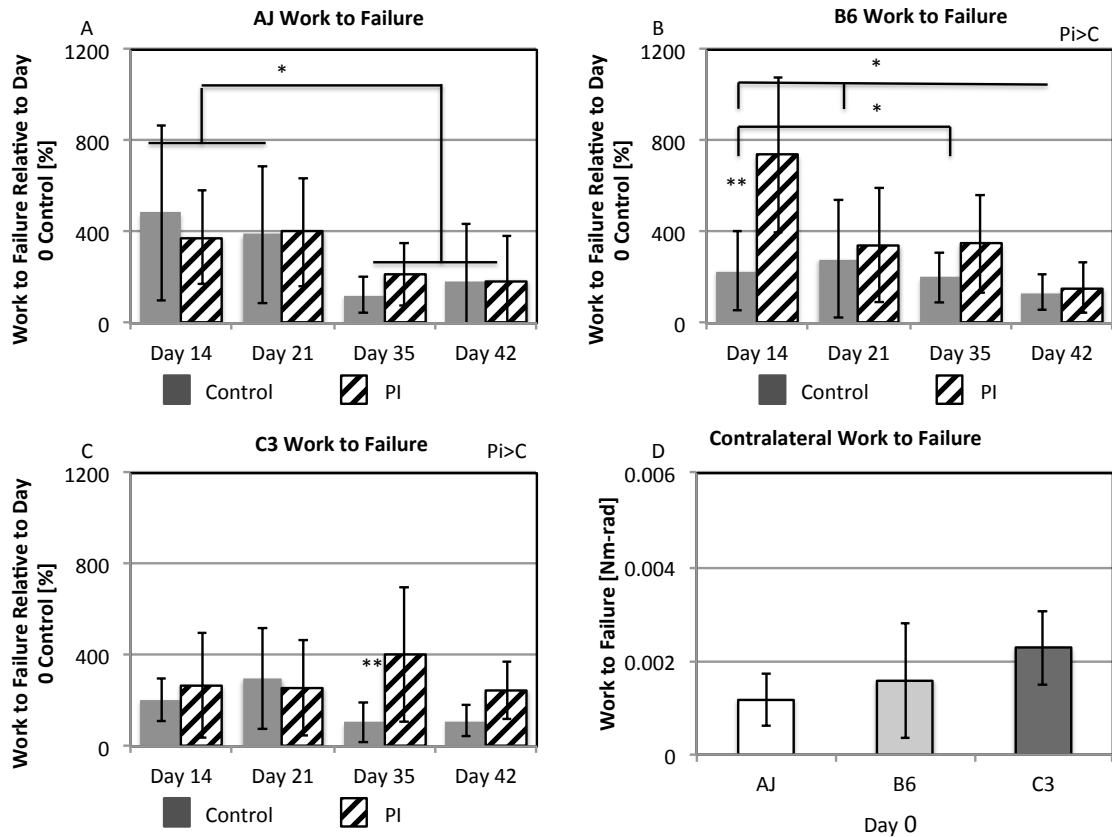


Figure 26. Work to Failure in Strains AJ, B6, and C3. A,B,C) All values are plotted as percentages of Day 0 control, non-fractured mice femora. Contralateral values are included for reference. * above horizontal lines signifies an interaction with POD. Significantly different results are separated by vertical lines. Significant differences due to diet effects are indicated on figure. ** above specific day signifies an interaction between POD and diet. D) Contralateral limb values at day 0 for work to failure.

Twist to failure is a measure of the angular displacement required to break a bone. Variations in twist to failure are demonstrated in Figure 27. In all strains twist to failure is greater at earlier points in time, but recovers to control, non-fractured values by POD 35. Overall dietary effects on twist to failure are only seen in B6 mice with Pi-deficient mice having a greater twist to failure than control mice. However, both B6 and C3 strains show specific interactions between the dietary perturbation albeit at different times. B6 mice have a dietary interaction earlier in time at POD 14 whereas this interaction in C3 mice is seen later at POD 42.

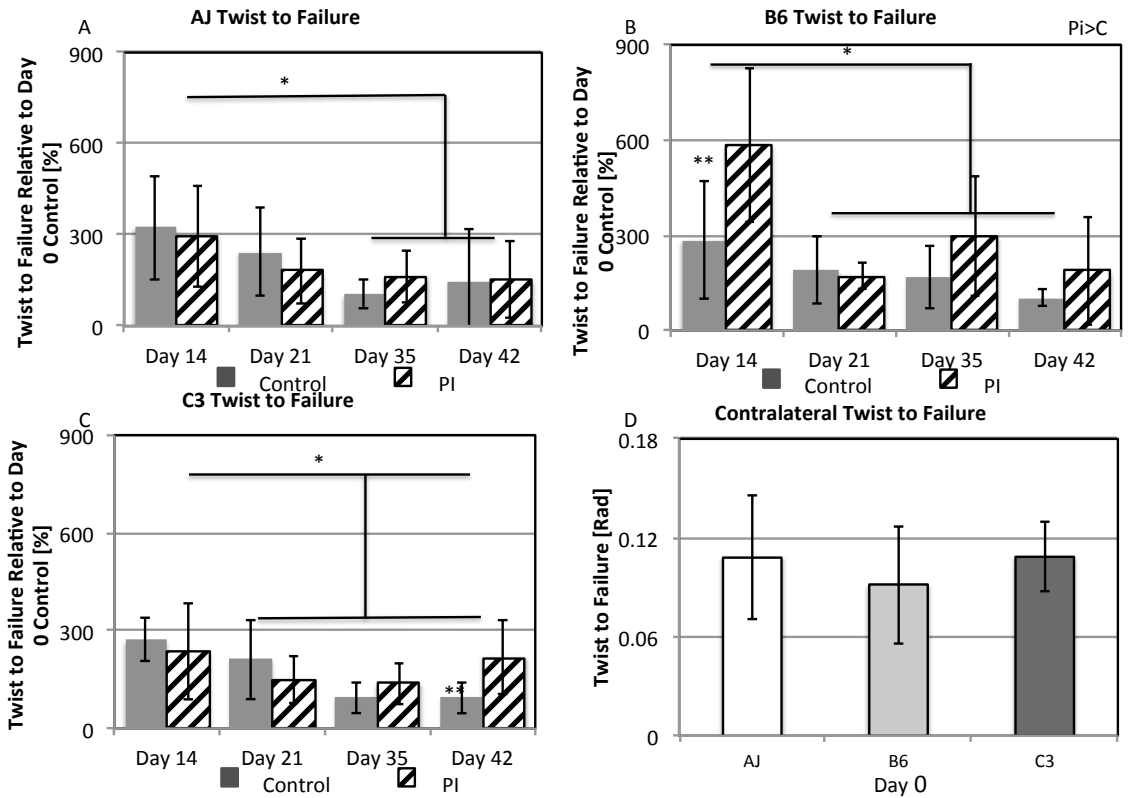


Figure 27. Twist to Failure for Strains AJ, B6, and C3. All values are plotted as percentages of Day 0 control, non-fractured mice femora. Contralateral values are included as a reference. * above horizontal lines signifies an interaction with POD. Significantly different results are separated by vertical lines. Significant differences due to diet effects are indicated on figure. ** above specific day signifies an interaction between POD and diet.

Stiffness is the last measurement of mechanical integrity discussed. It is measured in terms of both stiffness and rigidity and using two different areas of the torsion curve—narrow and break. Rigidity is more standardized because it factors out individual differences in bone length. Measures of stiffness (Figures 28 and 29) and rigidity (Figures 30 and 31) are provided below. Both stiffness and rigidity show a general trend of increasing over time. In all strains stiffness and rigidity are

lowest at POD 14. By POD 42 stiffness and rigidity have nearly returned to control, non-fractured values. Overall dietary effects are only seen in the B6 strain where, unlike the aforementioned mechanical properties, control mice show greater stiffness and rigidity than Pi-deficient mice (Figures 28, 30, and 31). The notable exception to this in B6 mice is stiffness measured using the entire torque-deformation curve (Figure 29).

Specific dietary interactions with post-operative time points are only seen when the stiffness is measured using the entire torque-deformation curve (Figure 29). Both AJ and B6 strains show a significant dietary interaction at POD 21, where Pi-deficient mice have greater stiffness than mice fed the control diet. The C3 mice show this dietary interaction at a later point in time, POD 35. Like stiffness measurements rigidity also shows specific dietary interactions, but only when measured using the entire curve (Figure 31). The only specific dietary interaction is seen in AJ mice at POD 21 at which point the Pi-deficient group has greater rigidity. This dietary interaction disappears by the two later time points.

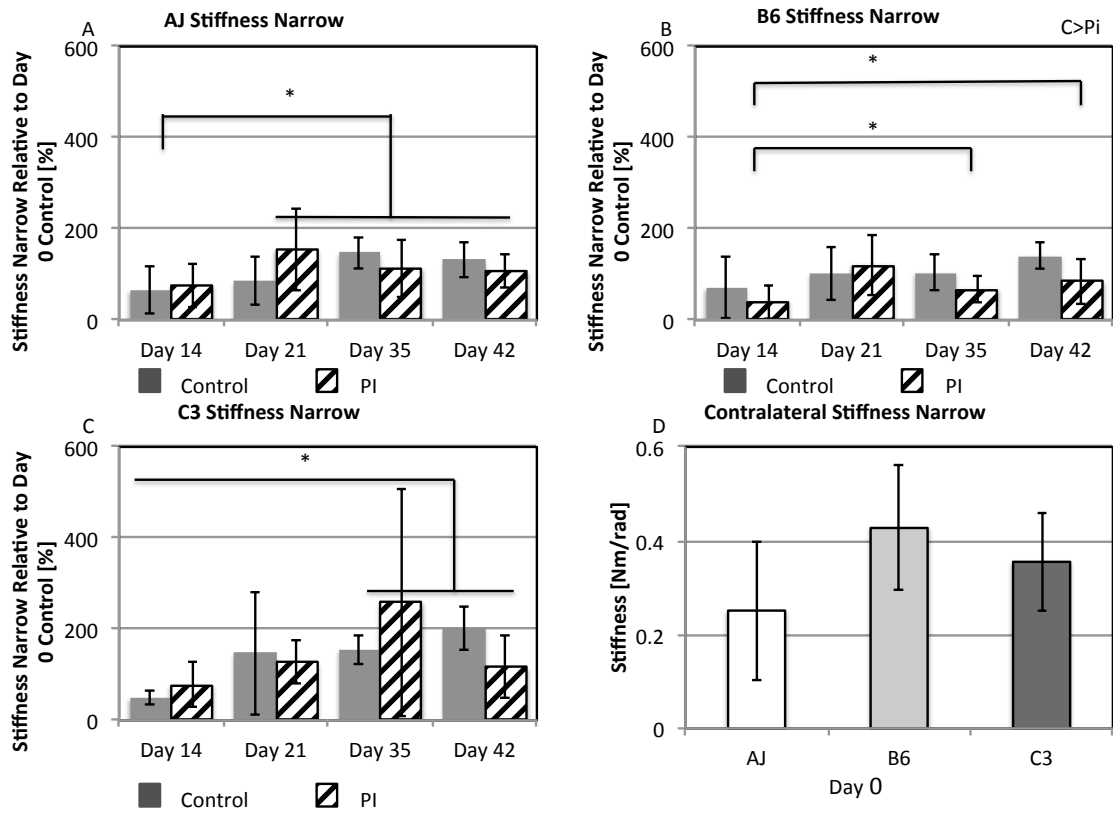


Figure 28. Stiffness Narrow for Strains AJ, B6, and C3. All values are plotted as percentages of Day 0 control, non-fractured mice femora. Contralateral values are included as a reference. * above horizontal lines signifies an interaction with POD. Significantly different results are separated by vertical lines. Significant differences due to diet alone are indicated on figure. ** above specific day signifies an interaction between POD and diet.

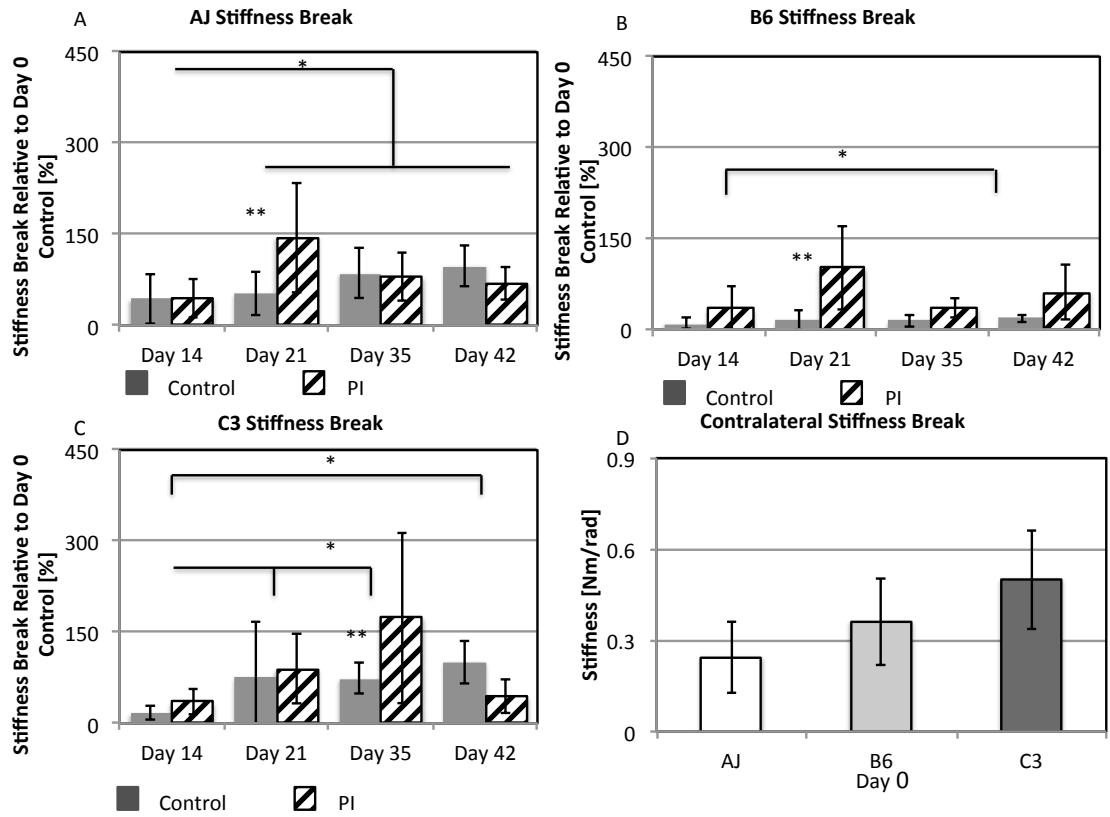


Figure 29. Stiffness Break for Strains AJ, B6, and C3. A,B,C) All values are plotted as percentages of Day 0 control, non-fractured mice femora. Contralateral values are included as a reference. * above horizontal lines signifies an interaction with POD. Significantly different results are separated by vertical lines. Significant differences due to diet effects are indicated on figure. ** above specific day signifies an interaction between POD and diet. D) Contralateral limb values at day 0 for stiffness break.

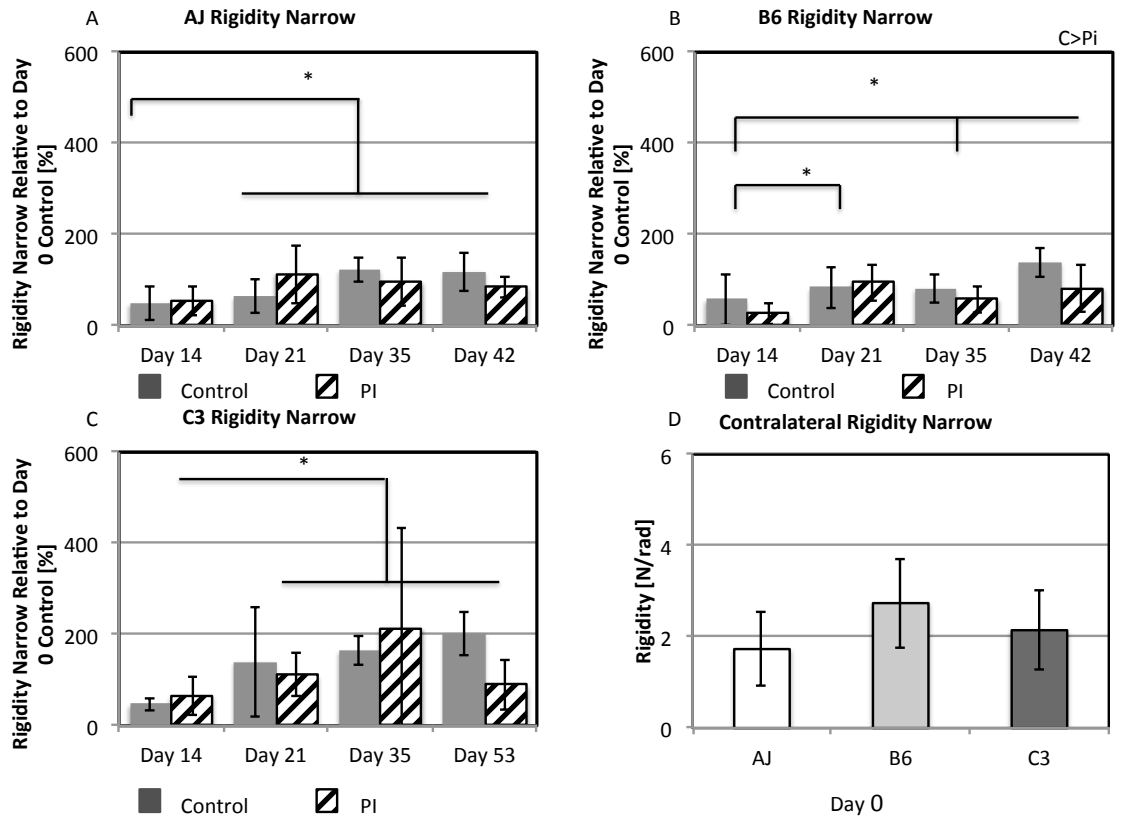


Figure 30. Rigidity Narrow for Strains AJ, B6, and C3. A,B,C) All values are plotted as percentages of Day 0 control, non-fractured mice femora. Contralateral values are included as a reference. * above horizontal lines signifies an interaction with POD. Significantly different results are separated by vertical lines. Significant differences due to diet effects are indicated on figure. ** above specific day signifies an interaction between POD and diet. D) Contralateral limb values at day 0 for rigidity narrow.

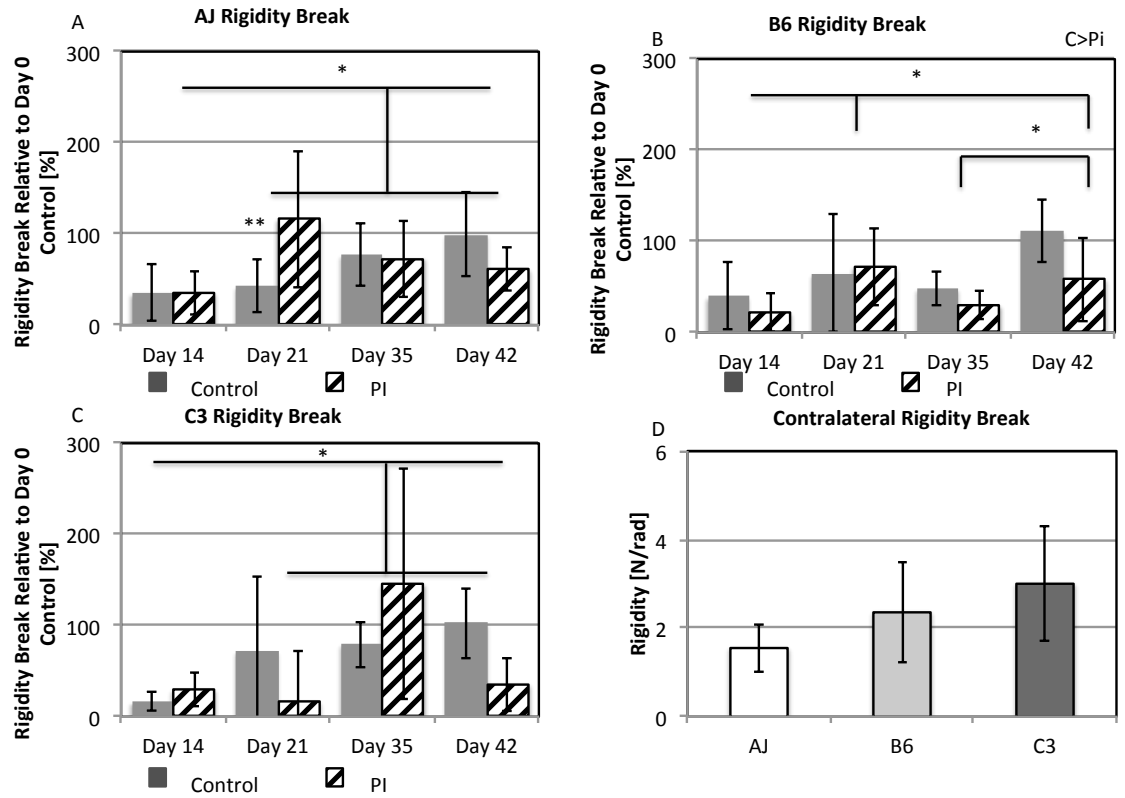


Figure 31. Rigidity Break for Strains AJ, B6, and C3. A,B,C) All values are plotted as percentages of Day 0 control, non-fractured mice femora. Contralateral values are included as a reference. * above horizontal lines signifies an interaction with POD. Significantly different results are separated by vertical lines. Significant differences due to diet effects are indicated on figure. ** above specific day signifies an interaction between POD and diet. D) Contralateral limb values at day 0 for rigidity break.

Discussion

The goal of this study was to determine the relationships between microstructural features of fracture callus tissues and the relative regain in mechanical properties. These studies then assessed how hypophosphatemia during the initial 14 days of endochondral bone formation affected these properties and the regain in mechanical function.

Overall Findings

All three strains showed statistically significant decreases in average gap length and porosity across all time points that were examined. These observations over time are consistent with a continuous progression in the microstructural integrity preceding throughout post-operative day 42 that was examined. The bridging cortices become more intact with the progression of time and have greater bridging at early time points in control calluses compared to calluses of mice fed a phosphate-restricted diet. This greater amount of bridging was evidenced by the lesser amount of porosity and smaller average gap size in the outer callus cortices. However, relatively few microstructural properties with the exception of tissue mineral density (TMD) show over 95% relative regain in integrity. This is in contrast to mechanical properties which all return to nearly 100% of pre-fracture values by post-operative day 42. Two notable exceptions to this 100% regain in pre-fracture values are B6 phosphate-deficient mice in the realms of “break” rigidity and stiffness. Mechanical properties tend to have an increase in value at earlier time points when compared to day 0 non-fractured control limbs and subsequently

return to a roughly equivalent value. Not all parameters are affected by diet and many of these parameters have significant differences only at specific points in time usually occurring either very early at post-operative day 14 or at post-operative day 21. These findings suggest that once phosphate has been replenished in the diet the effects due to phosphate restriction are reversible. Hypophosphatemia had an effect on all three strains of mice at post-operative day 14, but all three strains also showed reversibility once the phosphate had been replenished.

Callus Ring Properties

Post-operative day 42 consistently has the highest bone volume fraction across strains, indicating that as callus volume decreases, bone volume begins to increase as the callus becomes progressively more mineralized. This is consistent with the findings that across all three strains bone volume fraction increases with the progression of time. AJ mice show a significant difference in bone volume fraction of the ring with control callus rings having a greater bone volume fraction than phosphate-deficient callus rings. There is an interaction between diet and time in AJ mice that show a significantly increased bone volume fraction in control callus rings at post-operative day 42 when compared to phosphate-deficient callus rings. This may suggest that bone volume fraction in AJ mice is affected differently than their B6 and C3 counterparts and that this interaction between dietary perturbation and time becomes significant when the callus is nearly completely healed. In all three strains average gap size was significantly higher at POD 14 than the three later

time points, which suggests a rapid closure of the callus gaps by POD 21. This was specifically evident at the earliest time point in callus formation—post-operative day 14—when the chondrogenic period is more active than the osteogenic period, suggesting a role for phosphate in the early stages of bone remodeling. Also of note in regards to bone volume fraction is the period at which C3 mice are affected by diet. Taken altogether it appears that phosphate deficiency takes effect during the point in bone remodeling in which chondrogenesis is transitioning to osteogenesis. Bone volume fraction is very closely related to porosity, which represents the fraction of the callus that is non-mineralized tissue. Porosity decreases over time, consistent with the finding that bone volume fraction increases over time. This decrease in porosity also suggests that the bridging of the outer callus cortices becomes more intact with the progression of bone remodeling and healing. The porosity measurement is particularly useful at both post-operative day 14 and post-operative day 42, where interaction between dietary perturbation and time is evident. The AJ and B6 strains show similarities in that both strains have a statistically significant difference in porosity with phosphate-deficient calluses having a greater porosity than calluses of mice fed the control diet. Both AJ and B6 strains show interactions between dietary effects and post-operative time point at post-operative day 14. Phosphate-deficient callus rings show higher porosity than those of control calluses. In the AJ strain this interaction dissipates, suggesting the reversibility of dietary restriction once phosphate has been replenished. B6 strains, however, show an additional interaction at post-operative day 42 where phosphate-

deficient calluses once again have a greater porosity than control calluses, suggesting that phosphate deficiency may have a lingering effect on porosity in the B6 strain. Reciprocal relationships are seen in bone mineral density. BMD increases with the progression of time. However, in the AJ strain dietary restriction and time interact at post-operative day 42 where control calluses show greater BMD than phosphate-deficient calluses. This suggests that AJ mice are affected by dietary restrictions differently than their B6 and C3 counterparts and that this effect is seen once the callus has nearly completely healed. Tissue mineral density (TMD) takes into account only the mineralized tissue above certain strain-specific gray scale intensities, but does not include any tissue below these intensities. Both the AJ and B6 mice show statistically significant differences in callus TMD at post-operative day 14, which suggests that phosphate restriction has effects early in the bone remodeling process, but once phosphate is replenished in the diet these effects dissipate.

Regain in Microstructural Properties

All microstructural measurements for the fractured limbs were calculated as a percentage of non-fractured contralateral limbs in order to assess the regain in the microstructural integrity of fractured limbs compared to non-fractured control limbs without a dietary perturbation. Across all strains total volume shows a significant difference with the earlier time points (14 and 21) having nearly seven times as much volume as controls with later points (35 and 42) being reduced in total volume. By post-operative day 42 total volume was still shown to be over three

times as high as the non-fractured limbs. Bone volume fraction consistently increased across time points toward 100% of control value indicating that by post-operative day 42 there was a significant trend towards full bone volume fraction recovery. B6 mice had the lowest regain in bone volume fraction, reaching less than 70% of original control values. None of the strains showed dietary effects in regain of bone volume fraction. A trend towards increasing recovery of bone mineral density was observed across all three strains with variability in the particular regain in BMD for each strain. C3 mice and AJ mice show the fullest regain in BMD when compared against control values, with regain values in the 80% range. B6 mice do not show the same amount of regain in BMD, only reaching less than 70% when compared to controls. TMD is perhaps a better indicator of regain in microstructural integrity with all three strains reaching approximately 95% of control values. It is of note that all three strains show a decrease in TMD at post-operative day 21. This could signify an important transition in the bone remodeling process. More significant dietary effects on density are seen in TMD where both B6 and C3 mice have significant differences in TMD due to dietary effects. B6 and C3 mice have a consistently higher TMD in mice fed a phosphate-deficient diet compared to those who were fed a control diet. Because the phosphate-deficient mice also show a smaller bone volume at this particular point in time the increase in density of the tissue indicates a compensatory effect to maintain mechanical stability despite a decrease in mineralized tissue volume.

Mechanical Properties and Regain in Strength

A high degree of variability in individual animals is seen across all measurements in mechanical properties; however, this variability decreases as the animals approach post-operative day 42 and the fractured limbs approach 100% of the mechanical properties of non-fractured control limbs. It is of note that earlier stages in the bone repair process differ from later points in time, specifically post-operative days 35 and 42. Overall bone strength is a function of geometry and material composition. Differences in bone diameter occur at different points in the bone healing process and can account for the greater value of some mechanical parameters at earlier and intermediate points in time when the total volume is greater. These time points are of note because by post-operative day 42 mice mechanical properties have achieved almost a 1:1 ratio with those of non-fractured control limbs, indicating that the regain in mechanical strength is achieved by this point in time. In terms of specific mechanical properties both AJ and B6 showed the highest level of maximum torque at post-operative day 21 while C3 mice have the highest level of maximum torque later in the bone remodeling process at post-operative day 35. Maximum torque was greater in phosphate-deficient mice at both time points suggesting a possible compensatory response in the strength of the phosphate-deficient bones. In both the AJ and B6 strains the maximum torque in the diet restriction group returned to control levels suggesting that the ability of the

material to sustain a given rotational force return to normal levels once phosphate has been replenished in the diet, but this return to normal mechanical strength takes a considerable amount of time. In C3 mice the phosphate restriction effects are seen at an even later point in time at post-operative day 35. However, by post-operative day 42 the phosphate-restricted group does return to control levels with a total regain in maximum torque. Work to fracture is the bone's overall resistance to fracture and takes into account not only the maximum torque, but stiffness as well. Work to failure decreases over time in all three strains with a trend towards achieving a normal 1:1 correlation with non-fractured limbs. This logically follows the trend that stiffness increases over time as well. Twist to failure is defined as the amount of deformation that occurs before the bone fails. Twist to failure shows many variations in strain-specific sensitivity to diet perturbations. While the AJ strain does not show any statistically relevant dietary effects, B6 shows a significant effect at post-operative day 14 at which point the twist to failure in the phosphate-deficient group is twice as high as the control fractured limbs and six times as much as control non-fractured limbs. This suggests a very strong compensation in mechanical integrity at early points of phosphate restriction, which is rapidly lost upon phosphate replenishment. The C3 strain reveals a spike in twist to failure at post-operative day 42 among the phosphate-deficient mice. This is of note because it is possible that there is a spike in gene expression of osteogenic transcription factors after phosphate is replenished in the diet. This would be consistent with the observation that C3 mice show a prolonged chondrogenic period followed by a

rapid burst of osteogenesis (Hussein et al. 2015). Stiffness is defined as the extent to which a material resists deformation under an applied force—torsion in this instance. Stiffness increases at later post-operative days in all strains of mice, indicating that there is an increase in bone stiffness over time. It is of note that the diet restriction effects were only statistically significant in the B6 mice, but in all three strains it was evident that control calluses consistently showed a greater stiffness than those of their phosphate-restricted counterparts. By post-operative day 42 the phosphate-restricted groups remained at a lower stiffness than controls indicating that there may be a long-lasting effect in stiffness due to the phosphate-restriction. Rigidity, a mechanical parameter similar to stiffness but controls for the length of the sample, shows similar trends to those observed in stiffness measurements with an increase over time and B6 mice being the only strain to show an overall dietary effect.

Significance and Future Outlook

Because many microstructural properties of the tissue including bone volume fraction, bone mineral density, and tissue mineral density show a trend of increasing over time these increases may be correlated with a return to normal mechanical strength values. Additionally, measures of empty space such as average gap size and porosity show a decreasing trend over time. However, correlations between regain in microstructural properties and mechanical strength reveal that microstructural properties may not show the same extent of regain to pre-fracture values as

mechanical strength, or perhaps that these microstructural properties are further delayed in their return to pre-fracture values. The microstructural properties may continue to change even as the callus has been completely resorbed and secondary bone formation is occurring. The change in microstructural properties suggests a dynamic process that in turn affects the mechanical integrity of the structure. The mechanical properties fluctuate but do not show the same general increasing or decreasing trend because oftentimes the mechanical properties of the bone are highest at the mid-point (post-operative day 21) as the bone appears to go through what is an overshoot in mechanical strength most likely due in part to an increase in callus volume occurring at this same time point. But what specifically is happening on a genetic level at this time point to cause such a dramatic increase in mechanical strength, particularly in phosphate-deficient mice remains to be seen. Additionally strain differences were observed in the data but were not shown to be statistically different from each other, which suggests that the sample size was not sufficient to show a significant difference. Testing of more samples in the future may yield more statistical significances and further elucidate correlations between microstructural and mechanical properties. This study allows us to better understand the healing that occurs across time on the microstructural and mechanical level. The microstructural progressions that were observed in this study along with the advances in CT imaging technology will allow clinicians to better assess the degree of return to normal strength based on imaging data.

References

- Bonnarens, F, and TA Einhorn. Production of a standard closed fracture in laboratory animal bone. *Journal of Orthopaedic Research* 1984;2(1):97–101.
- Boron, WF and EL Boupaep. *Medical Physiology* (2nd ed.). Philadelphia: Saunders/Elsevier. 2012.
- Colnot, C, and T. Alliston. “Tissue interactions in long bone development.” In F Bronner, MC Farach-Carson, and HI Roach (eds.) *Bone and Development*, Pp. 25–37. London: Springer-Verlag. 2010.
- Hayward, LN et al. MRT letter: Contrast-enhanced computed tomographic imaging of soft callus formation in fracture healing. *Microscopy Research and Technique* 2012; 75(1):7–14.
- Hayward, LN et al. Assessment of contrast-enhanced computed tomography for imaging of cartilage during fracture healing. *Journal of Orthopaedic Research* 2013;31(4):567–573.
- Hussein, A et al. Genetic Variability in Fracture Healing Under Phosphate Deficiency. American Society for Bone and Mineral Research, 2015. Poster M00027.
- Hussein, AI et al. The effect of phosphate deficiency on callus composition. American Society for Bone and Mineral Research, 2014. Poster SU0067.
- Jepsen, KJ et al. Genetic randomization reveals functional relationships among morphologic and tissue-quality traits that contribute to bone strength and fragility. *Mammalian Genome* 2007;18(6–7):492–507.
- Jepsen, KJ et al. Genetic variation in the patterns of skeletal progenitor cell differentiation and progression during endochondral bone formation affects the rate of fracture healing. *Journal of Bone and Mineral Research* 2008;23(8):1204–1216.
- Jepsen, KJ et al. Establishing biomechanical mechanisms in mouse models: Practical guidelines for systematically evaluating phenotypic changes in the diaphysis of long bones. *Journal of Bone and Mineral Research* 2015;30(6):951–966.
- Kakar, S et al. Enhanced chondrogenesis and Wnt signaling in PTH-treated fractures. *Journal of Bone and Mineral Research* 2007;22(12):1903–1912.
- Lybrand, K et al. Delay in fracture healing by phosphate restriction displays uniform recovery in AJ and C57B6 strains independent of genetic variability. American

Society for Bone and Mineral Research, 2014. Poster MO0184.

Mescher, AL (ed.) *Junquiera's Basic Histology: Text and Atlas* (13th ed.) New York: McGraw Hill Medical. 2013.

Morgan, EF et al. Micro-computed tomography assessment of fracture healing: Relationships among callus structure, composition, and mechanical function. *Bone* 2009; 44(2):335–344.

Nyman, JS et al. Quantitative measures of femoral fracture repair in rats derived by micro-computed tomography. *Journal of Biomechanics* 2009;42(7):891–897.

Parsons, CA et al. Interspecies synteny mapping identifies a quantitative trait locus for bone mineral density on human chromosome Xp22. *Human Molecular Genetics* 2005;14(21):3141–3148.

Wigner, NA et al. Acute phosphate restriction leads to impaired fracture healing and resistance to BMP-2. *Journal of Bone and Mineral Research* 2010;25(4):724–733.

CURRICULUM VITAE

Erin K. Simmons
75 Beechcroft St. #1, Brighton MA 02135
eksimmonsbu@gmail.com (310) 569-1897
Year of Birth: 1991

EDUCATION

Boston University School of Medicine 2014-Expected May 2016
Candidate for Master of Science in Medical Sciences

Boston University
Bachelor of Arts in Neuroscience and English, with Honors May 2013

RESEARCH

Laboratory, Department of Orthopedics September 2015-Present
Boston University School of Medicine Dr. Louis C. Gerstenfeld

- Investigated the microstructural properties of fracture calluses in three different murine strains
- Determined the regain in microstructural properties and whole-bone mechanical properties in three different murine strains
- Data collection using micro-computed tomography and mechanical torsion testing

Harbor-UCLA Medical Center November 2013-August 2014
Clinton Kakazu, MD

- Participated in a clinical research team lead by Dr. Clinton Kakazu that investigated regional anesthesia techniques. Research topics included: pneumothorax, supraclavicular block, regional anesthesia technique for patients undergoing upper arm Arteriovenous Fistula formation, and historical perspectives on the use of adenosine for stent deployment.
- Shadowed physicians in the Department of Anesthesia.

WORK EXPERIENCE

EMT—Fallon Ambulance September 2015-Present

- I am responsible for the care, transport, and treatment of both emergent and non-emergent patients.

EMT Field Internship

August 2015

- Completed over 75 hours in the field working with patients under the supervision of senior Emergency Medical Service providers with McCormick Ambulance and the Los Angeles County Fire Department. Working as part of a team that administered high quality medical care to patients in the pre-hospital setting.

English Literature Tutor

October 2013-August 2014

- Helped students improve writing, grammar, and literature analysis skills.
- Prepared supplemental curriculum for students in disadvantaged academic circumstances or those who desired additional improvement.

Clinical Volunteer at Cedars-Sinai Medical Center November 2013-August 2014

- Assisted nurses and doctors in administrative tasks related to pre-operative care.
- Communicated and coordinated with operating room staff.
- Provided emotional support to patients undergoing anxiety.

Tutor for AP Biology

Fall 2011

- Conducted private tutoring sessions with a student at Brookline High School preparing to take the AP Biology Examination.

Teaching Assistant for Introduction to Biology

Spring 2011

Boston University

- Assisted Boston University students in proper lab techniques.
- Answered questions pertaining to biology subject matter.
- Led and conducted laboratory sessions on neuroanatomy.

PUBLICATIONS**A Diffusion Model Analysis of Reaction Times in Two-Choice Auditory Decision Tasks in Rats.** May 2013

- In this undergraduate honors thesis I investigated the application of Ratcliff's Diffusion Model to reaction times of perceptual decisions using auditory stimuli. This model was used to elucidate a change in decision mechanism with practice—an indication of the cognitive processes that accompany long-term learning. Published in the Undergraduate Research Opportunity Program Journal.

In the Era of Ultrasound Guidance, Is Pneumothorax from Supraclavicular Block a Thing of the Past? March 2014

- This paper discusses zero incidence of pneumothorax in over 1400 patients—one of the largest patient populations in this area. This study demonstrated statistically significant results for zero incidence of pneumothorax using ultrasound-guided supraclavicular block. In addition, we discuss the theoretical long-term risks of acquiring a pneumothorax using the data collected at Harbor-UCLA Medical Center.

PERSONAL

- Volunteer on a medical mission to Honduras with the Boston University Global Medical Brigades
- Recognized as the featured student of the Boston University Department of English
- Volunteer at Los Angeles Harbor Animal Shelter
- Lector at Saint John Fisher Catholic Church